Accepted Manuscript

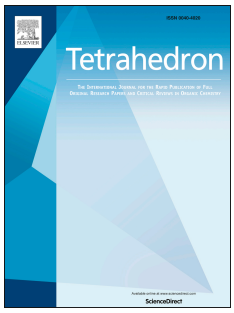

Soft Ruthenium and Hard Brønsted Acid Combined Catalyst for Efficient Cleavage of Allyloxy Bonds. Application to Protecting Group Chemistry

Shinji Tanaka, Yusuke Suzuki, Hajime Saburi, Masato Kitamura

PII: S0040-4020(15)00598-0

DOI: 10.1016/j.tet.2015.04.088

Reference: TET 26691

To appear in: *Tetrahedron*

Received Date: 12 March 2015

Revised Date: 22 April 2015

Accepted Date: 24 April 2015

Please cite this article as: Tanaka S, Suzuki Y, Saburi H, Kitamura M, Soft Ruthenium and Hard Brønsted Acid Combined Catalyst for Efficient Cleavage of Allyloxy Bonds. Application to Protecting Group Chemistry, *Tetrahedron* (2015), doi: 10.1016/j.tet.2015.04.088.

Graphical Abstract

To create your abstract, type over the instructions in the template box below.
Fonts or abstract dimensions should not be changed or altered.

Soft Ruthenium and Hard Brønsted Acid Combined Catalyst for Efficient Cleavage of Allyloxy Bonds. Application to Protecting Group Chemistry.

Leave this area blank for abstract info.

Shinji Tanaka, Yusuke Suzuki, Hajime Saburi, Masato Kitamura*
Graduate School of Pharmaceutical Sciences, Graduate School of Science, and Research Center for Materials Science, Nagoya University, Chikusa, Nagoya 464-8601, Japan

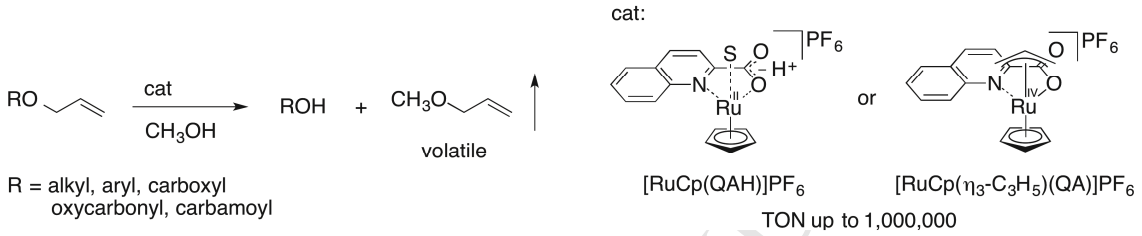

ELSEVIER

Tetrahedron
journal homepage: www.elsevier.com

Soft Ruthenium and Hard Brønsted Acid Combined Catalyst for Efficient Cleavage of Allyloxy Bonds. Application to Protecting Group Chemistry.

Shinji Tanaka[a], Yusuke Suzuki[a], Hajime Saburi[a], and Masato Kitamura[a]*

[a]*Graduate School of Pharmaceutical Sciences, Graduate School of Science, and Research Center for Materials Science, Nagoya University, Chikusa, Nagoya 464-8601, Japan*

ARTICLE INFO

Article history:
Received
Received in revised form
Accepted
Available online

Keywords:
Allyl Group
Deprotection
Ruthenium
Quinaldic acid
Catalysis

ABSTRACT

We show that a monocationic CpRu(II) complex of quinaldic acid (QAH) and a monocationic CpRu(IV)(π-allyl)QA complex catalyze efficient cleavage of the allyloxy bond in allyl ethers, allyl esters, allyl carbonates, and allyl carbamates in methanol without the need for additional nucleophiles. The only co-product is volatile allyl methyl ether, enhancing operational simplicity during isolation of the deprotected alcohols, acids, and amines. This clean and high-performance catalytic system should contribute to protecting group chemistry during the multistep synthesis of pharmaceutically important natural products. Full details of this system, including the mechanism, are reported.

1. Introduction

Protecting groups (PGs) are the unsung heroes or heroines of chemistry. This detail is barely acknowledged in the retrosynthetic analysis of complicated natural and unnatural products, but it would not be too strong to say that accomplishing total synthesis is impossible without PGs, even in the 21st century with its variety of highly sophisticated synthetic methods.[1] **Fig. 1** illustrates the general process for the protection of a function, **A**, in the conversion of **B** to **Z**. As is standard, **A** is first protected by a PG (red circle), and then the function **B** is subjected to a series of target reactions. Finally, **A** is deprotected by the action of reagents (black sphere) to give the desired product together with the co-product. High stability of the PG under various reaction conditions, as well as facile and chemoselective removal of the PG on demand, is essential. Furthermore, easy separation of the excess reagent and accompanying co-product from the desired product is also required. These requirements become even more stringent during the synthesis of polar biomolecular compounds such as peptides, nucleotides, and polysaccharides.

Among more than a thousand PGs invented so far, we have revisited the allyl (All) group for protecting an alcohol as an allyl ether, which has a structure as simple as that of an acetyl group and has higher stability toward both acidic and basic conditions. This chemical stability, however, often causes difficulty in

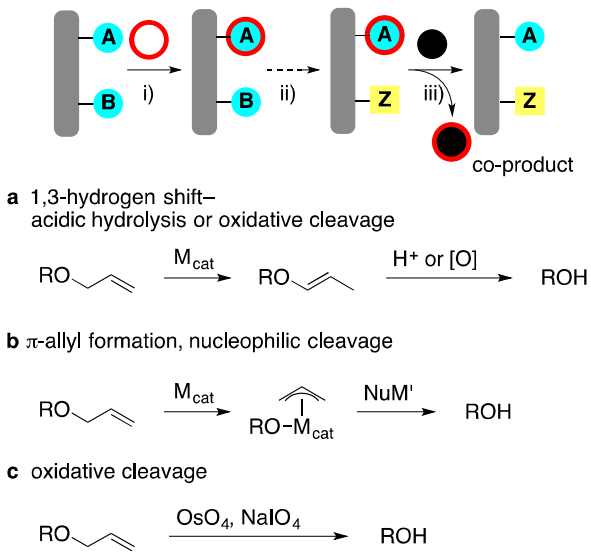

Fig. 1. Protecting group (PG) chemistry and the utility of allyl PG for alchols in organic synthesis. i) Protection. ii) Target function transformation from **B** to **Z**. iii) Deprotection. Red circle: protecting group. Black sphere: reagent for deprotection. Black sphere in red circle: co-product.

* Corresponding author. Tel.: +0-000-000-0000; fax: +0-000-000-0000; e-mail: author@university.edu

deprotection or deallylation under mild conditions. As shown in **Fig. 1a**, the most popular approach to deprotection is Corey's method:[2] $RhCl(P(C_6H_5)_3)_3$ catalyzes a 1,3-hydrogen shift of the allyl ether to the corresponding alkenyl ether, which is then either hydrolyzed under acidic conditions or oxidatively cleaved. $[Ir(P(C_6H_5)_2(CH_3))_2(cod)]PF_6$ reported by van Boom in 1980 shows higher catalytic performance.[3] The types of one-step deprotection shown in **Fig. 1b** and **Fig. 1c** are simple, and many methods have been invented on the basis of Tsuji's Pd π-allyl chemistry,[4] Ni π-allyl chemistry,[5] and Os-catalyzed oxidative cleavage.[6]

A major disadvantage common to all of these methods is that an excess amount of acids, bases, oxidizing reagents, or reducing reagents is required, complicating the reaction system. The ideal approach would clearly be the "*No additive, One step*," process shown in **Fig. 1b**, but such a catalytic system has not been attained. We therefore aimed to develop an optimal process that performs direct cleavage of the allyl ether under very mild conditions, and ultimately attained a monocationic CpRu(II) complex of quinaldic acid (QAH) and a monocationic CpRu(IV)(π-allyl)QA complex. The present article describes full details of the screening results establishing $CpRu^+$/QAH-catalyzed deallylation/allylation[7] and a mechanistic study of this process.

2. Results and discussion

2.1. Catalyst design concept

We previously established a leading concept for the design of a molecular catalyst, "intramolecular metathesis-type donor-acceptor bifunctional catalyst" (Intramol-MDACat), via the detailed mechanistic study of catalytic asymmetric 1,2-addition of diorganozincs to aldehydes.[8] This concept realized a new type of asymmetric reaction including reduction,[9] 1,4-addition of diorganozincs to enones,[10] and others.[11] Furthermore, the Intramol-MDACat concept has been extended to "Intermol-MDACat" and to a "soft transition metal/hard Brønsted acid-combined catalyst" to achieve the efficient asymmetric hydrogenation of β-keto esters.[12]

With this approach in mind, we designed a concept catalyst for allyloxy bond cleavage on the basis of a "intramolecular redox-mediated donor–acceptor bifunctional catalyst" (Intramol-RDACat), as shown in **Fig. 2**. Here, the central transition metal M(*n*) is coordinated by $\mathbf{L_s}$–$\mathbf{L_h}$H ($\mathbf{L_s}$, soft ligating atom; $\mathbf{L_h}$, hard ligating atom) and a monoanionic and highly electron-donative η^5 cyclopentadienyl (Cp) ligand, endowing the M complex with a soft coordination site and a hydrogen-bond donor site. In this soft M/hard H^+ combined system, the hard oxygen atom of an allyl ether substrate would interact with H^+, while the soft C=C double bond would coordinate to M as a η^2 ligand. Enhancement of the electrophilicity or acceptability of the allyl moiety synergistically cooperates with the high nucleophilicity or donicity of the CpM(*n*) moiety, thereby facilitating movement of the substrate/catalyst complex to a δ^+-δ^--δ^+-δ^--δ^+-δ^- charge-alternating transition state involving M(*n*) oxidation. Such stabilization of the transition state would result in easy generation of the corresponding π-allyl CpM(*n* + 2) moiety. In addition, introduction of Cp and the bidentate property of $\mathbf{L_s}$–$\mathbf{L_h}$H should prevent self-aggregation of the catalyst, which often causes catalyst deactivation. Lastly, if the π-allyl complex can react with CH_3OH, which could be used as a possible solvent, the CpM($\mathbf{L_s}$–$\mathbf{L_h}$H) catalyst would be regenerated alongside liberation of the deprotected alcohols and allyl methyl ether (CH_3OAll) as the co-product, which could be easily removed simply by evaporation. This concept catalyst would be applicable to allyl esters, allyl carbonates, and allyl carbamates.

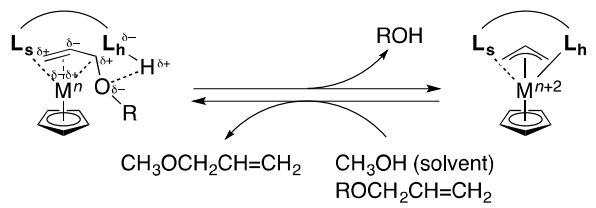

Fig. 2. Concept catalyst designed on the basis of "intramolecular redox-mediated donor-acceptor bifunctional catalyst (Intramol-RDACat)." $\mathbf{L_s}$: soft ligating atom. $\mathbf{L_h}$: hard ligating atom.

2.2. Screening of $\mathbf{L_s}$–$\mathbf{L_h}$H ligands

Initially, the central metal was selected as Ru(II) in $[RuCp(CH_3CN)_3]PF_6$ (**1**) on the basis of our finding in 2002 that $[RuCp(P(C_6H_5)_3)(CH_3CN)_2]PF_6$ prepared from **1** and $P(C_6H_5)_3$ catalyzes the allyloxy bond cleavage of allyl esters.[13] The catalyst screening was combinatorially conducted by using the customized automated synthesizer Chemspeed,[14–15] which has five reaction blocks each containing 16 reaction vessels, and can be used under an inert Ar atmosphere. Forty-eight commercially available ligands L1–L48 (except for L36), used in a combination of $\mathbf{L_s}$ (sp^3P, sp^2N, sp^3N, and others) with $\mathbf{L_h}$H (COOH, OH, NH_2, and no proton), were screened simultaneously under the following ideal conditions for alcohol deprotection: $[C_6H_5$-$CH_2CH_2OCH_2CH=CH_2$ ($C_6H_5CH_2CH_2OAll$ (**2**))] = 100 mM; [**1**] = 1 mM; [$\mathbf{L_s}$–$\mathbf{L_h}$H] = 1 mM; solvent, CH_3OH; 30 °C; 3 h. The Chemspeed system automatically mixed the CH_3OH solutions of the $\mathbf{L_s}$–$\mathbf{L_h}$H ligands, **1**, and $C_6H_5CH_2CH_2OAll$ (**2**) in the reaction vessels, and sampled the reaction mixtures in a programed way. GC analysis was used to determine the yields of deprotected alcohol **3** and 1,3-hydrogen shift side product **4** (column, DB-WAX (0.25 mm x 15 m) as follows: temp., 50 °C + 10 °C/min; t_R, 6.0 min (**2**), 4.0 min (**3**), and 4.5 min (**4**)). **Fig. 3** shows the results. 2-Pyridinecarboxylic acid (PAH; PA indicates 2-pyridinecarboxylate) quantitatively afforded **3**. 8-Hydroxyl quinoline derivatives also showed some acceleration effect. Sulfides and azoles showed almost no reactivity, and phosphines tended to isomerize the allyl group to the corresponding alkenyl ether **4**.

As shown in **Table 1**, the ligand structure–reactivity relationship was further investigated by shortening the reaction time to 1 h using the particularly highly reactive PAH as the starting point (entry 1). Neither pyridine nor benzoic acid, nor a 1:1 mixture of pyridine and benzoic acid showed an acceleration effect (entries 2–4). No reaction proceeded when the location of COOH in PAH was changed from C(2) to C(3) or C(4) (entries 5 and 6) or when H^+ was removed from PAH as PANa (sodium 2-picolinate) or $PACH_3$ (methyl 2-piclolinate) (entries 7 and 8). Replacement of the carboxyl group with a hydroxymethyl or aminomethyl group also resulted in no reaction, although a proton is located in the same position as the carboxyl group (entries 9 and 10). Quinoline-8-carboxylic acid, in which the sp^2N atom and H^+ are located in a 1,6 manner rather than the 1,5 manner of PAH, showed no reactivity (entry 11). The presence of an electron-withdrawing substituent at the C(4) position of the pyridine ring of PAH tended to increase the reactivity with values of 27% (4-CH_3O), 39% (4-H), 50% (4-Cl), 54% (4-CF_3), and 59% (4-NO_2) (entries 1 and 12–15). Introduction of $PO(OH)_2$ (pK_a ca. 1.5) instead of COOH (pK_a ca. 5.4) in PAH enhanced the reactivity; however, further increasing the acidity by replacing COOH with SO_3H (pK_a ca. –3) resulted in deceleration (entries

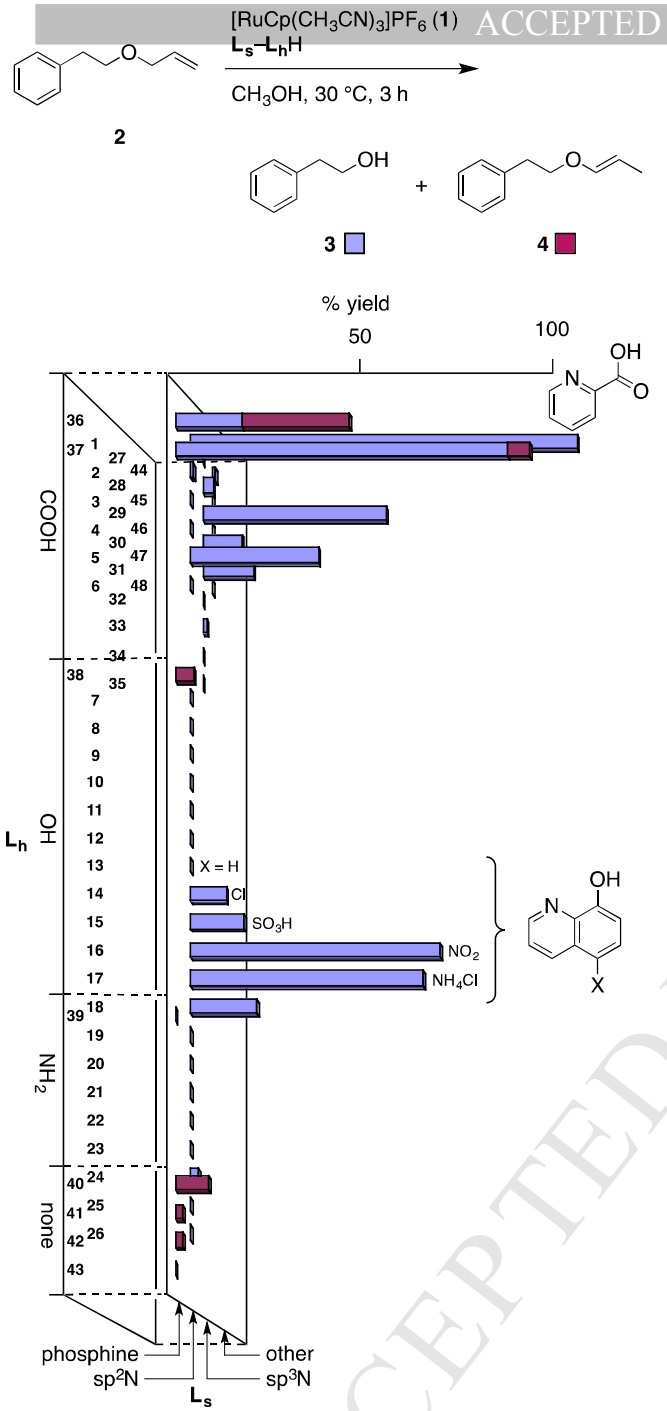

Fig. 3. Screening of $\mathbf{L_s}$–$\mathbf{L_h}$H under ideal conditions of [**2**] = 100 mM; [**1**] = 1 mM; [$\mathbf{L_s}$–$\mathbf{L_h}$H] = 1 mM; CH_3OH; 30 °C; 3 h. The x-coordinate shows the functional group of $\mathbf{L_h}$ moiety. "None" indicates no functional group. The y-coordinate corresponds to $\mathbf{L_s}$ moiety such as sulfide, azole, amine, pyridine, and phosphine. The vertical axis shows the % yields of the products (light blue-colored bar for the desired phenylethyl alcohol (**3**), and the purple bar for the undesired 1,3-hydrogen shift product (**4**). The structures of efficient ligands were drawn in the graph. For the structures of other ligands, see Experimentals. The numbers 1–48 in the graph correspond to L1–L48.

16 and 17) (*vide infra*). Fusion of a benzene ring at C(3)/C(4) or C(4)/C(5) of PAH led to deceleration, while the most impressive enhancement in reactivity was attained with quinaldic acid (QAH, 2-quinolinecarboxylic acid; QA indicates 2-quinolinecarboxy-late), in which a benzene ring is fused at C(5) and C(6) of PAH (entries 18–20): in this case, the reaction was completed within 1 h. The results in **Table 1** clearly indicate

Table 1. Ligand structure-reactivity relationship in the deallylation of $C_6H_5CH_2CH_2OAll$ (**2**) to $C_6H_5CH_2CH_2OH$ (**3**) using $[RuCp(CH_3CN)_3]PF_6$ (**1**)[a]

Entry	Ligand	Yield %[b]	Entry	Ligand	Yield %[b]
1	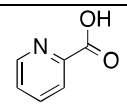	39 (80)	11[c]	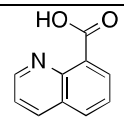	0
2[c]		0	12	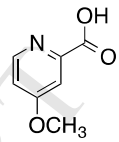	27 (70)
3[c]	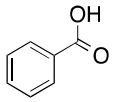	0	13	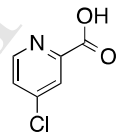	50 (91)
4[c]	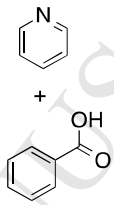	0	14	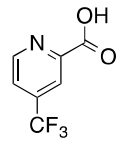	54 (95)
5[c]	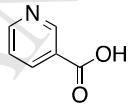	0	15	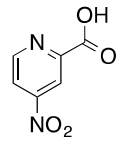	59 (96)
6[c]	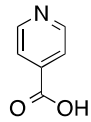	0	16	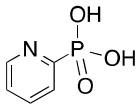	63 (92)
7[c]	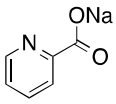	0	17	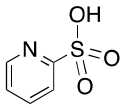	24 (31)
8[c]	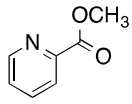	0	18	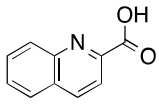	97 (99)
9[c]	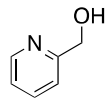	0	19	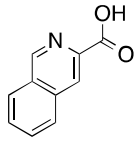	18 (48)
10[c]	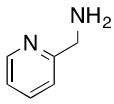	0	20	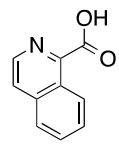	12 (43)

[a]Conditions: [**2**] = 500 mM; [**1**] = [ligand] = 1 mM; solvent, CH_3OH; temperature, 30 °C; 1 h.
[b]Values in parentheses are obtained after 3 h.
[c][**2**] = 100 mM.

the importance of i) a synergetic effect between the sp^2N atom and the adjacent COOH group, producing a five-membered chelating ring with the monocationic CpRu(II) catalyst precursor;

Table 2. Optimization of deallylation conditions using QAH/[RuCp(CH_3CN)$_3$]PF_6 (**1**), [RuCp(η^3-C_3H_5)(QA)]PF_6 (**5**), or PAH/CpM precursors

Entry	Metal Precursor	Ligand	**1**, mM	S/C	Solvent	Time, h	Yield %[b]
1	[CpRu(CH_3CN)$_3$]PF_6	QAH	100	100	CH_3OH	0.5	>99
2	[CpRu(CH_3CN)$_3$]PF_6	QAH	500	500	CH_3OH	3	99[c]
3	[CpRu(CH_3CN)$_3$]PF_6	QAH	1000	1000	CH_3OH	3	98[d]
4	[CpRu(η^3-C_3H_5)(QA)]PF_6	—	3000	10000	CH_3OH	24	99[e]
5	[CpRu(CH_3CN)$_3$]PF_6	QAH	100	100	C_2H_5OH	2	99
6	[CpRu(CH_3CN)$_3$]PF_6	QAH	100	100	*i*-C_3H_7OH	3	98
7	[CpRu(CH_3CN)$_3$]PF_6	QAH	100	100	*t*-C_4H_9OH	13	82
8	[CpRu(CH_3CN)$_3$]PF_6	QAH	100	100	1:1 CH_3OH –H_2O	6	99
9	[CpRu(CH_3CN)$_3$]PF_6	QAH	100	100	1:1 CH_3OH –DMF	6	99
10	[CpRu(CH_3CN)$_3$]PF_6	QAH	100	100	1:1 CH_3OH –THF	0.5	99
11	[CpRu(CH_3CN)$_3$]PF_6	QAH	100	100	1:1 CH_3OH –CH_2Cl_2	0.5	99
12	[CpRu(CH_3CN)$_3$]PF_6	QAH	100	100	1:1 CH_3OH –CH_3CN	3	18
13	[MoCp(CO)$_3$]$_2$	PAH	100	100	CH_3OH	3	0
14	[WCp(CO)$_3$]$_2$	PAH	100	100	CH_3OH	3	0
15	[FeCp(CO)$_3$]$_2$	PAH	100	100	CH_3OH	3	0
16	RhCp(cod)	PAH	100	100	CH_3OH	3	0
17	IrCp(cod)	PAH	100	100	CH_3OH	3	0

[a]Unless specified otherwise, all of reactions were carried out at 30 °C.
[b]GC analysis.
[c]2-g scale.
[d]Under a reduced pressure of 200 mmHg.
[e]The pressure of the reaction system was reduced to ca. 200 mmHg for 5 min every 2 h.

ii) the acidity of the proton; and iii) the molecular orbital coefficient of the ligand (see Mechanism).

2.3. Optimization

Table 2 showed the results of optimization of the standard reaction (**2** → **3**) using QAH and **1**, and other Cp metal precursors. The QAH/**1**-combined system was highly reactive, completing the reaction within 30 min (entry 1). Even with a substrate/catalyst (S/C) ratio of 500, deprotection was achieved in 3 h (entry 2). Under a slightly reduced pressure (200 mmHg), the S/C ratio could be increased to 1000 (entry 3). Further enhancement in the reactivity was realized by using a π-allyl complex, [RuCp(η^3-C_3H_5)(QA)]PF_6 (**5**), which was quantitatively prepared as a pale yellow solid from **1**, QAH, and allyl alcohol (AllOH) in an exact 1:1:1 ratio (**1** and QAH, acetone, rt, <5 min; addition of AllOH, rt, 15 min; concentration of the mixture to 1/10 volume).[7c] The complex **5** is air- and moisture-stable, which increases operational simplicity. Even with a 0.01 mol% of **5** (S/C = 10000), the reaction could be completed at 30 °C in 24 h by reducing the pressure to ca. 200 mmHg at 2-h intervals (entry 4). Removal of the co-product allyl methyl ether (CH_3OAll) would force the equilibrium toward the desired product side. In addition to CH_3OH, C_2H_5OH and *i*-C_3H_7OH could be used as solvents, whereas *t*-C_4H_9OH gave a lower yield (entries 5–7). Reactivity was maintained in CH_3OH containing H_2O, DMF, THF, or CH_2Cl_2 as a co-solvent. Using CH_3CN as a co-solvent significantly retarded the reaction (entries 8–12). Although our investigations of the central metal were limited, CpMo, CpW, CpFe, CpRh, and CpIr precursors—which are known to form π-allyl complexes—were not effective under the standard conditions using PAH (entries 13–17).

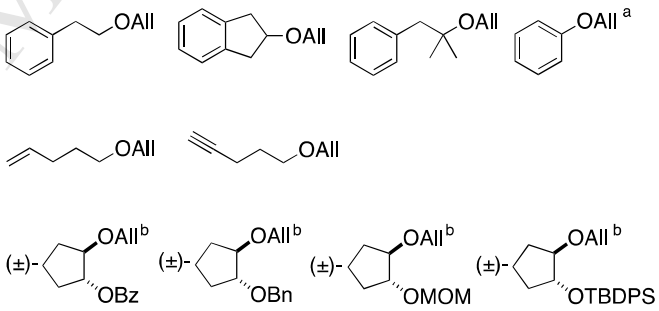

Fig. 4. Quantitative removal of allyl group from various allyl ethers at 30 °C for 3 h in CH_3OH with S/C ratio of 500 unless specified otherwise. [a]S/C = 100. [b]S/C = 100 and 0.5 h. All = $CH_2CH{=}CH_2$. Bz = COC_6H_5. Bn = $CH_2C_6H_5$. MOM = CH_2OCH_3. TBDPS = Si(*t*-C_4H_9)(C_6H_5)$_2$.

2.4. Generality

Fig. 4 summarizes the generality of the CpRu/QAH-catalyzed deprotection of alcohols from allyl ethers.[7a–7c] Primary, secondary, and tertiary alkanols, and phenol were quantitatively deprotected. No Claisen rearrangement occurred with allyl phenyl ether. Both allyl 4-pentenyl ether and allyl 4-pentynyl ether were quantitatively converted to the corresponding alcohol without, respectively, isomerization of the terminal olefin to an internal olefin or inhibition from the terminally alkyne. Benzoate, benzyl ether, methoxymethyl ether, and *tert*-butyldiphenylsilyl ether were not affected at all, realizing selective removal of allyl group.

As shown in **Fig. 5**, the present catalytic allyloxy bond cleaver could be used for allyl esters including carbonates, carboxylates, and phosphates.[7e] Allyloxycarbonyl (AOC)-protected alcohols showed much higher reactivity than other esters: a turnover number of one million was attained by continuous removal of

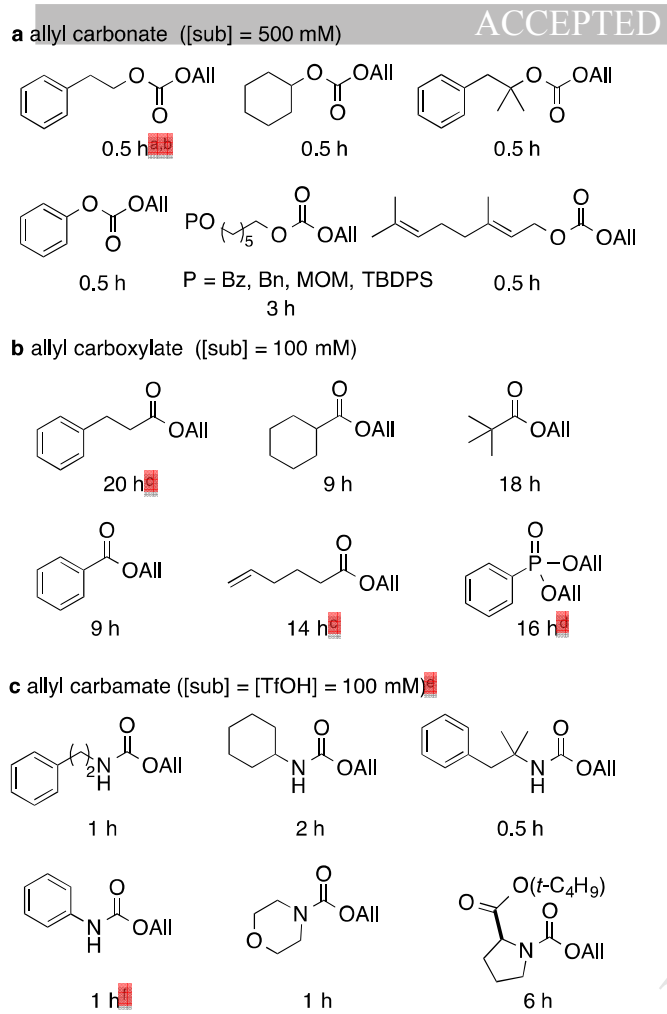

Fig. 5. Quantitative removal of allyl group from various allyl esters at 30 °C in CH_3OH with S/C ratio of 500 unless specified otherwise. The value is the reaction time. [a]10-g scale.[7e] [b]9 days with S/C ratio of 1.0 x 10^6. [c]*i*PrOH instead of CH_3OH. [d]500 mM. [e]S/C = 100. [f]88% yield.

volatile CH_3OAll. For diallyl carbonates, only less substituted allyl groups were selectively removed. Amines protected as an *N*-AOC group were efficiently deprotected in the presence of a 1-mol amount of CF_3SO_3H to give the corresponding ammonium salt without any *N*-allylated side product.[7d] The effectiveness of isolation could be amplified by salt formation. A 1-mol amount of Nafion (SO_3H equivalent), CH_3SO_3H, and 12 M aqueous HCl could be used, whereas a 10-mol amount of CH_3COOH was required for efficient cleavage.

The "*No additive-One step*" allyl cleaver functions smoothly without requiring an excess amount of reducing reagents, acids, bases, or oxidizing reagents, which often complicate the process of isolating the products. Therefore, the CpRu/QAH-combined catalyst can be applied to peptide synthesis and to the final deprotection stage in the synthesis of polar biomolecular compounds. Some examples are shown in **Fig. 6**. Highly multi-functionalized molecules, such as *N*-Fmoc-(*S*)-Glu(OAll)-O*t*Bu, *N*-Fmoc-(*S*)-Phe-(*S*)-Glu(OAll)-O*t*Bu, *N*-Fmoc-(*S*)-Ser(OAll)-(*S*)-Phe-O*t*Bu, 2'-OAll uridine, *N*-AOC-(*S*)-Pro-O*t*Bu, and *N*-AOC-(*S*)-Pro-(*S*)-Pro-Gly-O*t*Bu, were quantitatively deallylated without affecting the *t*Bu ester or Fmoc groups and without loss of reactivity, even in the presence of a highly coordinative peptide linkage.[7a,7d,7e] An RNA-related molecule—fully allyl-protected 3,5-U—was also converted in one step to 3,5-U, which was then isolated after $(C_2H_5)_3N$ addition.[7f] After the

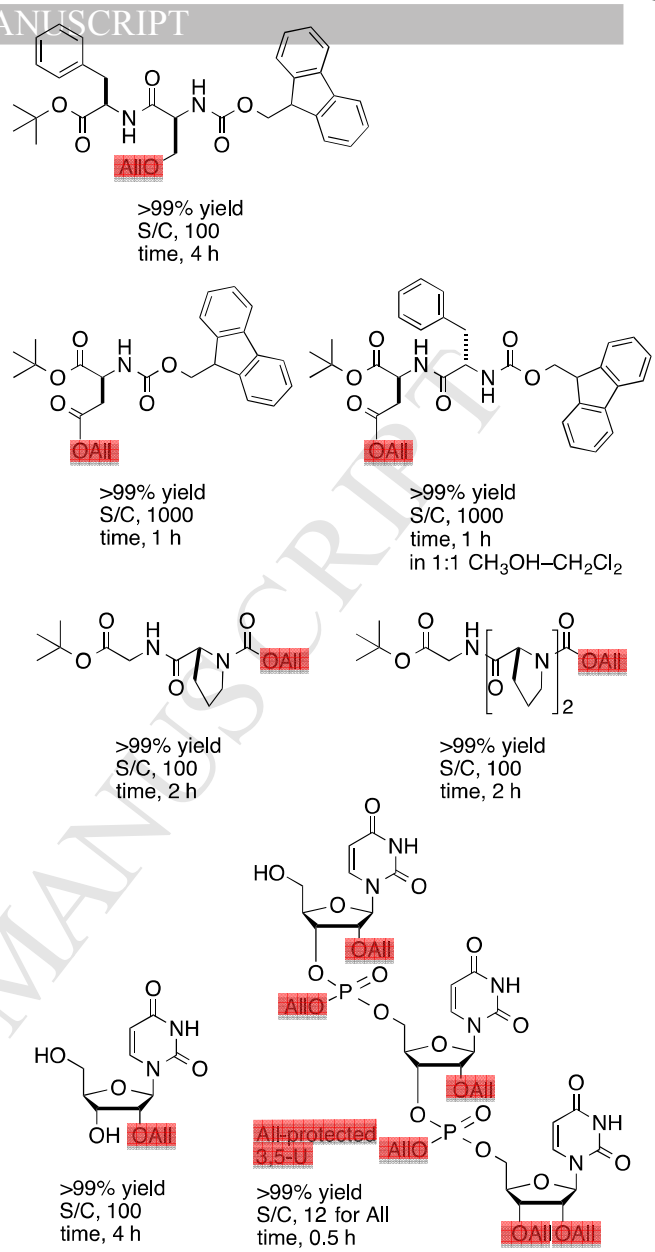

Fig. 6. Application to highly polar molecules. The deprotection yield as well as the conditions are shown below the substrate structure.

deprotection process, a catalyst sometimes ends up as an impurity in the final product. In this regard, a homogeneous catalyst is disadvantageous in comparison to its heterogeneous counterpart. The heterogeneous deallylation catalyst **6** immobilized on micro-size spherical SiO_2 particles containing Fe_3O_4 should be all the more practical because it can operate in alcoholic solvents in the absence of extra additives and the only co-product is volatile CH_3OAll. Products can be easily isolated through a simple deprotection step, followed by magnetic separation of **6**, and an evaporation process. 3,5-U was successfully deprotected by using the heterogeneous version of the catalyst.[7h]

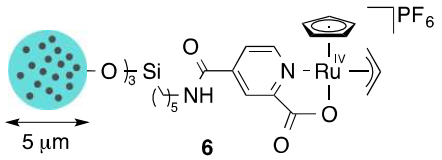

2.5. Mechanism

2.5.1. NMR study and kinetics

Fig. 7 shows the step-by-step changes in the ^{1}H-NMR spectrum during the reaction of QAH, $[RuCp(CH_3CN)_3]PF_6$ (**1**), CH_2=$CHCH_2OH$ (AllOH), $C_6H_5CH_2CH_2OAll$ (**2**), and CH_3OH in acetone-d_6 at 30 °C. When a 1-mol amount of **1** was added to a solution of QAH, the six aromatic proton signals of QAH completely and immediately disappeared to generate two new sets of relatively broad signals in a 20:1 ratio (**Fig. 7a** and **7b**). The major set could be plausibly assigned to $[RuCp(QAH)S]PF_6$ (**7**, S = CH_3CN or $(CD_3)_2CO$), while the minor one might be due to a species equilibrating with **7**—for example, [RuCp(QA)S] (**8**)/HPF_6 or a COOH-dangling complex **9** (for supposed structures, see **Fig. 11**).

Consistent with such a dynamic system, both the major and minor signals were converted to a single set of sharp signals when a 1-mol amount of **2** was introduced (**Fig. 7c**). The new signals could be definitely assigned to the π-allyl complex $[RuCp(\eta^3\text{-}C_3H_5)(QA)]PF_6$ (**5**), in which the π-allyl ligand takes an *endo* conformation to Cp, as supported by the observation of 2% and 4.5% nOe enhancement between the closely located CpH and the anti-protons H_A and $H_{A'}$ of the π-allyl group.[7b] The

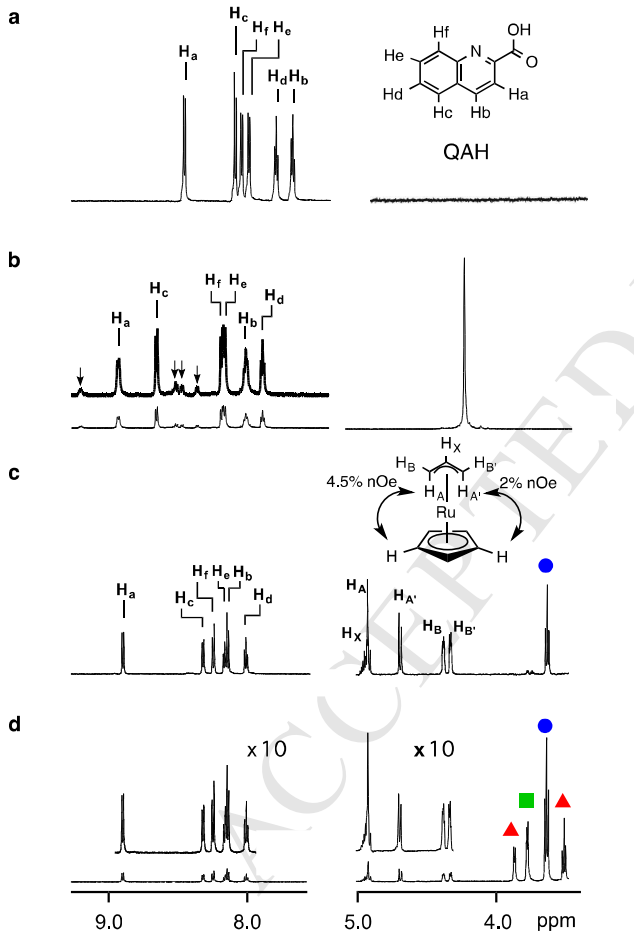

Fig. 7. ^{1}H-NMR behavior in the reaction of QAH with $[RuCp(CH_3CN)_3]PF_6$ (**1**), $C_6H_5CH_2CH_2OAll$ (**2**), and CH_3OH (acetone-d_6, 30 °C). (a) Quinaldic acid (QAH) (10 mM). (b) 10 min after addition of 1 mol amount of **1**. (c) 30 min after addition of 1 mol amount of **2**. The structure of QA moiety in the spectrum is omitted. (d) 12 h after addition of 10 mol amounts of **2** and 100 mol amounts of CH_3OH. Blue sphere: $C_6H_5CH_2CH_2OH$ (**3**). Red triangle: $C_6H_5CH_2CH_2OAll$ (**2**). Green square: CH_3OAll. All = CH_2CH=CH_2. The factor of OCH_2 signal intensity of CH_3OAll for **2** was ca. 0.5.

A_2B_2X signal pattern of the π-allyl ligand, rather than A_4X, indicates that the σ-π-σ exchange in **5** is slow on the ^{1}H NMR timescale. Stereoselective generation of *endo*-**5** can be explained by attractive interactions between π-allyl 1,3-p orbitals and Ru d_{xy}* and between π-allyl 2-p* orbital and Ru d_{z2}.[13b, 16]

The spectrum was not changed by the addition of a 1-mol amount of $C_6H_5CH_2CH_2OAll$ (**2**) into the solution of **5**. When 10-mol amounts of **2** and 100-mol amounts of CH_3OH were added to **5**, 70% of **2** was consumed after 12 h at 30 °C to generate $C_6H_5CH_2CH_2OH$ (**3**) and CH_3OAll in a 1:1 ratio (**Fig. 7d**). Here, only the π-allyl complex **5** was observed, showing i) that a π-allyl mechanism is operating; ii) that **5** is in the resting state of the catalytic cycle; and iii) that the rate is determined at the reductive nucleophilic attack of CH_3OH on the π-allyl C(1) or C(3) of **5** (see section 2.5.4).

The ^{1}H-NMR behavior agreed well with the kinetics shown in **Fig. 8**: the reaction proceeded with a 0th-order dependence on the initial concentration of $C_6H_5CH_2CH_2OAll$ (**2**) and with a 1st-order dependence on the initial concentration of the Ru complex **5** during the early stage of 0%–30% conversion of **2**.[15] Because both **2** and CH_3OAll act as an allyl donor, an excess amount of CH_3OH forced the equilibrium **2** + CH_3OH ⇆ **3** + CH_3OAll far to the right side. The 0.25:0.788:0.688:9.31 ratio of **2**, **3**, CH_3OAll, and CH_3OH observed in the ^{1}H-NMR spectrum (**Fig. 7d**) determined an equilibrium constant *K* of ca. 0.23, indicating that the **2** + CH_3OH side is preferred over the **3** + CH_3OAll side under the reaction conditions.

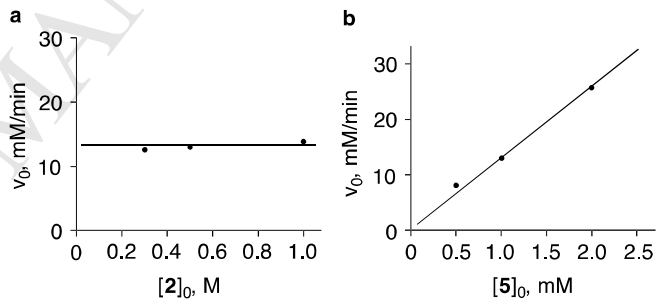

Fig. 8. Dependence of the initial rate v_0 (mM/min) on $[C_6H_5CH_2CH_2OAll$ (**2**)$]_0$ and $[[RuCp(\eta^3\text{-}C_3H_5)(QA)]PF_6$ (**5**)$]_0$ in the deallylation of **2** in CD_3OD at 30 °C. (a) Plot of v_0 as a function of $[2]_0$ from 300 mM to 1000 mM ($[5]_0$ = 1.00 mM). (b) Plot of v_0 as a function of $[5]_0$ from 0.500 mM to 2.00 mM ($[2]_0$ = 500 mM).

2.5.2. X-ray crystallographic analysis

The π-allyl complex **5** was air- and moisture-stable and easily crystalized from dichloromethane (yellow, prism, mp 166 °C (dec)).[7b] A series of π-allyl Ru complexes of 4-X-substituted picolinate (4-X-PA, where X = CH_3O, H, Cl, CF_3, and NO_2) were prepared, and the molecular structures in the crystalline state are shown in **Fig. 9**. In all cases, the π-allyl ligand had a conformation that was *endo* to the Cp group, being consistent with the structure of **5** in solution. The π-allyl C(3)–Ru bond was ca. 5% longer than the C(1)–Ru bond, albeit with a few exceptions. This observation indicates that the rate-determining reductive nucleophilic attack of CH_3OH may occur on the C(3) carbon.

2.5.3. Hammett plots and molecular orbital analysis

The relative reactivity of PAH for 4-X-PAH (X = CH_3O, Cl, CF_3, and NO_2) was investigated in the Ru-catalyzed deallylation of **2** to **3** under the conditions of [4-X-PAH] = [**1**] = 1 mM; [**2**] = 500 mM; CH_3OH; 30 °C). As shown in **Fig. 10a**, a stronger electron-withdrawing ability of X led to higher reactivity, but the

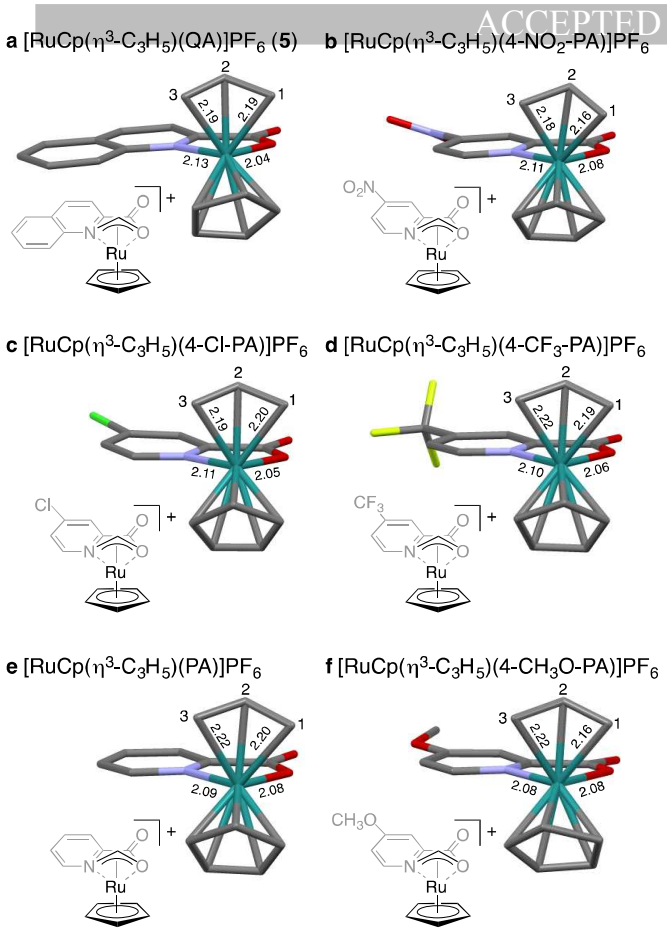

Fig. 9. Molecular structures of $[RuCp(\eta^3\text{-}C_3H_5)(QA)]PF_6$ (**a**) and $[RuCp(\eta^3\text{-}C_3H_5)(4\text{-}X\text{-}PA)]PF_6$ (**b**–**f**) in the crystalline state. QAH: quinaldic acid. 4-X-PAH: 4-X-substituted picolinic acid.

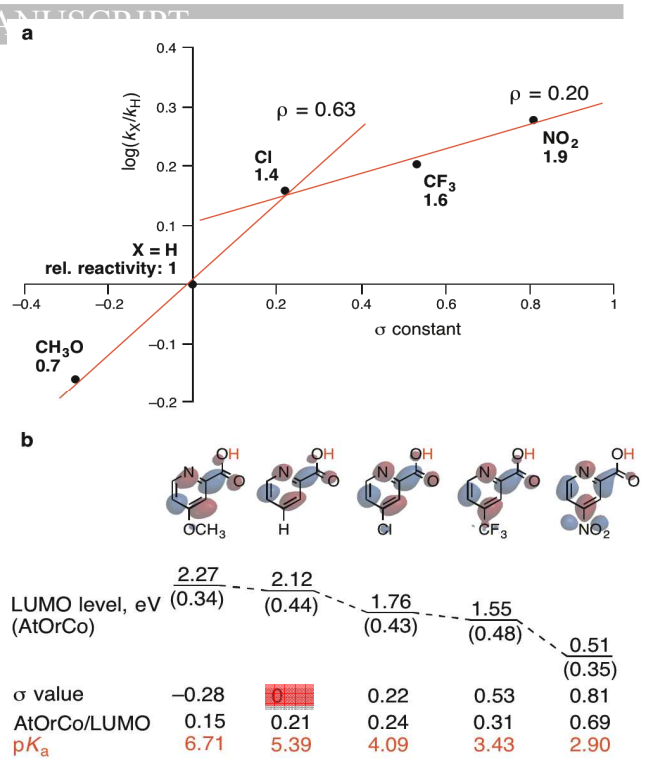

Fig. 10. Relationship between reactivity, LUMO energy level and acidity of 4-X-substituted picolinic acid (4-X-PAH) in deallylation of $C_6H_5CH_2CH_2OAll$ (**2**) to $C_6H_5CH_2CH_2OH$ (**3**) under the conditions of [**2**] = 500 mM; $[[RuCp(CH_3CN)_3]PF_6$ (**1**)] = [4-X-PAH] = 1 mM; CH_3OH; 30 °C. All = $CH_2CH{=}CH_2$. (a) Hammett plots of relative reactivity ($\log(k_X/k_H)$ as a function of standard σ constants. (b) LUMO energy calculated at a 6-31G* level, AtOrCo (atomic orbital coefficiency on N), and pK_a (COOH) of 4-X-PAH.

degree of rate enhancement was not as significant as expected: 0.7 (CH_3O, –0.28 (σ value)), 1 (H, 0.00), 1.4 (Cl, 0.22), 1.6 (CF_3, 0.53), and 1.9 (NO_2, 0.81). Hammett plots of $\log(k_X/k_H)$ versus the standard σ constant for the substituent parameter exhibited two linear free-energy relationships with a ρ value of +0.63 for X = CH_3O, H, and Cl, and +0.20 for X = Cl, CF_3, and NO_2, respectively. The two-line behavior may be rationalized by the balance between two factors: i) the π-accepting ability of the pyridine moiety, and ii) the acidity of the carboxylic acid of 4-X-PAH.[17] In the rate-determining reductive nucleophilic attack of CH_3OH on the π-allyl ligand of $[Ru(IV)Cp(\eta^3\text{-}C_3H_5)(4\text{-}X\text{-}PA)]PF_6$, a ligand with higher π-acceptability and a lower lowest unoccupied molecular orbital (LUMO) level should stabilize the transition state. This view is consistent with the LUMO level/reactivity relationship shown in **Fig. 10b**, and holds even after taking the atomic orbital coefficient (AtOrCo) of the nitrogen atom into consideration. As the AtOrCo/LUMO value decreases, the reactivity increases. π-Expanded QAH, which has a LUMO level 0.6 eV lower than that of PAH (2.12 vs 1.52), shows a reactivity that is 5–10-fold higher than PAH. At the same time, however, a strong electron-withdrawing group with a high σ value raises the acidity of COOH. The dibasic mono salt $[Ru(II)Cp(4\text{-}X\text{-}PAH)]PF_6$ may exist in equilibrium with the neutral complex [Ru(II)Cp(4-X-PA)] and HPF_6. The acidity of COOH in $[Ru(II)Cp(4\text{-}X\text{-}PAH)]PF_6$ would be enhanced by coordination of the COOH oxygen atom to the mono cationic central Ru atom, intensifying the acidity of COOH beyond expectation from the general p*K*a values of PAH (ca. 5.4) and HPF_6 (ca. –20). An increase in the generation of neutral species with no Intramol-RDACat ability is likely to lower the catalyst performance of the $CpRu(II)^+$/Brønsted acid-combined system. This would explain our observation that replacement of COOH in PAH with highly acidic SO_3H led to low reactivity (**Table 1**, entry 17).

2.5.4. Supposed catalytic cycle

On the basis of the results of the NMR study, kinetics experiments, structural analysis of Ru π-allyl complexes by X-ray diffraction, Hammett plots analysis, and molecular orbital calculation, the catalytic cycle of the present deallylation using the $[RuCp(CH_3CN)_3]PF_6$ (**1**)/QAH-combined system or $[RuCp(\eta^3\text{-}C_3H_5)(QA)]PF_6$ (**5**) was deduced, as shown in **Fig. 11**. First of all, CH_3CN in **1** is easily replaced with QAH to generate a mono cationic complex $[RuCp(QAH)S]PF_6$ (**7**), which is in equilibrium with both a neutral complex [RuCp(QA)S] (**8**)/HPF_6 and a COOH-dangling species $[RuCp(QAH)S_2]PF_6$ (**9**). The $Ru(II)^+/H^+$ in $[RuCp(QAH)S]PF_6$ captures an allyl ether substrate, $CH_2{=}CHCH_2OR$, to form the catalyst/substrate complex **10**, in which the hard ether O atom interacts with the hard H^+ ion, and the soft olefin double bond interacts with the soft Ru atom. The hydrogen bond in **10** enhances the electrophilicity of C(3) and C(1) in $CH_2{=}CHCH_2OR$, while the electron donicity or nucleophilicity of the central Ru atom is amplified by coordination of the carboxylate-like O atom, electron-donative sp^2N atom, and mono anionic η^5 Cp ligand. This synergetic effect realizes a charge alternation in H--O–C(1)–C(2)=C(3)-- Ru--OCO to reduce the energy level of the transition state. The Intramol-RDACat ability facilitates the oxidative formation of the *endo*-π-allyl complex **5**, liberating a deprotected alcohol. The rate-determining reductive nucleophilic attack of

CH_3OH on the π-allyl carbon is made easier by the lower LUMO energy of QAH, generating **11**. The CH_3OAll is then replaced with the substrate **2**, thereby completing the cycle. All elementary steps are reversible, but the presence of an excess amount of CH_3OH solvent rotates the cycle in a clockwise way. Removal of the volatile co-product by reducing the internal pressure or by purging the reaction mixture with an inert gas would result in an infinite turnover number.

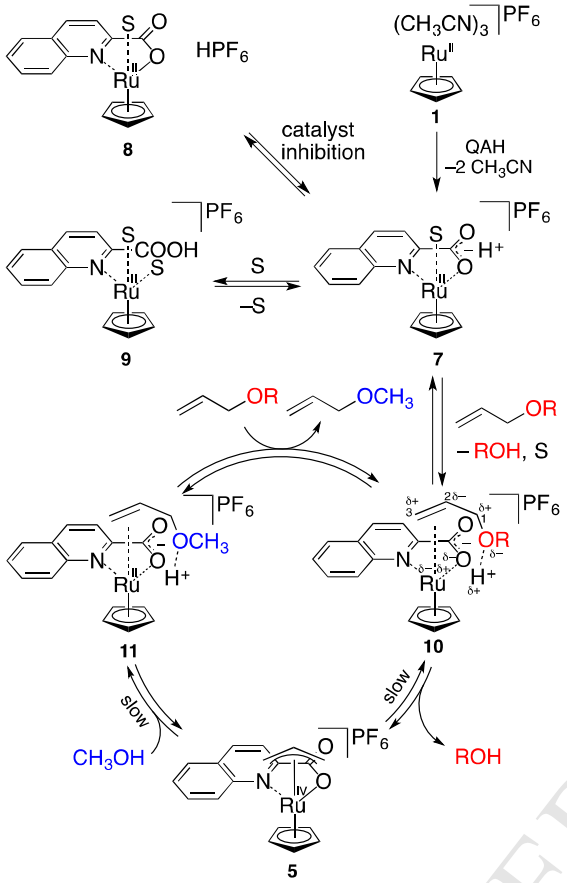

Fig. 11. Supposed catalytic cycle in deprotection of alcohols using $CpRu^+$/QAH-combined system. S = CH_3CN, CH_3OH, substrate, product, etc.

3. Conclusion

In summary, the $CpRuPF_6$-quinaldic acid catalyst described here functions as a highly reactive and chemoselective allyloxy bond cleaver in alcoholic solvents under very mild and essentially additive-free conditions. The only co-product is volatile ether. The efficiency and simplicity of the reaction should further increase the practical utility of allyl groups for the protection of alcohols, esters, and amines, among many other protecting groups in organic synthesis. Furthermore, the validity of our leading concept for designing the molecular catalyst—namely "soft transition metal/hard Brønsted acid-combined catalyst" or "redox-mediated donor-accepter bifunctional catalyst (RDACat)"—has been confirmed by a series of experiments including i) ^{1}H-NMR spectrometry; ii) X-ray crystallographic analyses of CpRu-π-allyl complexes of picolinic acid derivatives; iii) Hammett plot analysis; and iv) the relationship between LUMO levels of ligands and reactivity. The present study should stimulate further ideas, not only for the retrosynthetic design of pharmaceutically important natural and unnatural compounds, but also for the continued development of molecular catalysis.[18]

4. Experimental

4.1. General

A Chemspeed ASW2000 system was used to screen ligands. Nuclear magnetic resonance (NMR) spectra were recorded on a JEOL JNM-ECA-600 spectrometer. Chemical shifts are expressed in parts per million (ppm) downfield from tetramethylsilane or in ppm relative to $CHCl_3$ and CHD_2COCD_3 (δ 7.26 and 2.05 in ^{1}H NMR, and δ 77.0 and 29.8 in ^{13}C NMR). The signal patterns of ^{1}H NMR are indicated as follows: s, singlet; d, doublet; t, triplet; q, quartet; m, multiplet; and br, broad signal. X-ray crystallographic analysis was conducted on a Rigaku Saturn 70 CCD system, and the structure was solved by direct methods using CrystalStructure crystallographic software. Quantum chemical calculations were performed using the Spartan 10 program implemented on an Apple iMac 3.4 GHz intel core i7. Gas chromatography analyses were performed on a Shimadzu GC-17A instrument. Argon (Ar) gas was purified by passage first through a column of BASF R3-11 catalyst at 80 °C and then through a column of granular calcium sulfate. Solvents for the deallylation and the synthesis of Ru complexes were dried, degassed at reflux temperature in the presence of the following appropriate drying agents (250 mg/100 mL) under an Ar stream for 6 h, and distilled into Schlenk flasks: calcium hydride for *i*PrOH, CH_2Cl_2, CH_3CN and CD_3CN; magnesium for C_2H_5OH, CH_3OH and CD_3OD; sodium for hexane, benzene and benzene-d_6; and MS4A for acetone, acetone-d_6, $(CH_3)_2CDOH$ and $(CD_3)_2CDOD$. The solvent was degassed by three freeze–thaw cycles before deallylation. In a similar manner, diethyl ether, THF and THF-d_8 were distilled from sodium benzophenone ketyl (3 g/L). $CDCl_3$ was purchased from Cambridge Isotope Laboratories and purified by alumina column chromatography. It was degassed by three freeze–thaw cycles before use in the ^{1}H NMR study. All other solvents were obtained commercially and used without further purification unless stated otherwise.

Details for the deallylation procedure, the results of the allyloxy substrates in "section 2.4 on Generality," and the NMR data of the substrates and deprotected products have been reported in the supporting information of previous short communications.[7]

4.2. Ligand and CpM screening

4.2.1. Materials

Ligands L1–L48 shown in **Fig. 3** were as follows: picolinic acid (PAH, L1), hydroxy(pyridin-2-yl)methanesulfonic acid (L2), quinoline-8-sulfonyl chloride (L3), 1*H*-imidazole-4-carboxylic acid (L4), pyridine-2,6-dicarboxylic acid (L5), 1*H*-benzo[*d*]imidazole-2-sulfonic acid (L6), pyridin-2-ylmethanol (L7), 2-((dimethylamino)methyl)pyridin-3-ol (L8), (*Z*)-picolinaldehyde oxime (L9), 3*H*-[1,2,3]triazolo[4,5-*b*]pyridin-3-ol (L10), 1*H*-benzo[*d*][1,2,3]triazol-1-ol (L11), pyridin-2-ol (L12), quinolin-8-ol (L13), 5-chloroquinolin-8-ol (L14), 8-hydroxyquinoline-5-sulfonic acid (L15), 5-nitroquinolin-8-ol (L16), 5-(chloro-λ^5-azanyl)quinolin-8-ol hydrochloride (L17), 2-(benzo[*d*]oxazol-2-yl)phenol (L18), pyridin-2-ylmethanamine (L19), picolinamide (L20), [2,2':6',2"-terpyridin]-4'(1'*H*)-one (L21), 2-(pyridin-2-yl)-1*H*-benzo[*d*]imidazole (L22), 6-ethoxybenzo[*d*]thiazole-2-sulfonamide (L23), 1*H*-pyrazole-1-carboximidamide hydrochloride (L24), 2,2'-bipyridine (L25), pyridine (L26), glycine (L27), (*S*)-2-amino-3,3-dimethylbutanoic acid (L28), proline (L29), piperidine-2-carboxylic acid (L30), piperazine-2-carboxylic acid hydrochloride (L31), 1*H*-indole-2-carboxylic acid (L32), 1*H*-pyrrole-2-carboxylic acid (L33), dimethylglycine (L34), methyl-*L*-proline (L35), 2-(diphenyl-

phosphanyl)acetic acid (L36), 2-(diphenylphosphanyl)benzoic acid (L37), 2-(diphenylphosphanyl)ethan-1-ol (L38), 2-(diphenylphosphanyl)ethan-1-amine (L39), triphenylphosphane (L40), tricyclohexylphosphane (L41), (2-methoxyethyl)diphenylphosphane (L42), 2-(diphenylphosphanyl)-*N*,*N*-dimethylethan-1-amine (L43), 2-(4-oxo-2-thioxothiazolidin-3-yl)acetic acid (L44), thianthren-1-ylboronic acid (L45), 2-(thiophen-2-yl)acetic acid (L46), benzo[*b*]thiophen-2-ylboronic acid (L47), and furan-2-carboxylic acid (L48). Except for L36, all ligands were commercially purchased and used without further purification. L36 was synthesized according to a previously reported method.[19]

The ligands shown in **Table 1** were as follows: benzoic acid, nicotinic acid, isonicotinic acid, sodium picolinate, methyl picolinate, quinoline-8-carboxylic acid, 4-methoxypicolinic acid (4-CH_3O-PAH), 4-chloropicolinic acid (4-Cl-PAH), 4-(trifluoromethyl)picolinic acid (4-CF_3-PAH), 4-nitropicolinic acid (4-NO_2-PAH), pyridin-2-ylphosphonic acid ($PyPO(OH)_2$), pyridine-2-sulfonic acid ($PySO_3H$), isoquinoline-1-carboxylic acid, isoquinoline-3-carboxylic acid, quinoline-2-carboxylic acid (QAH). Except for $PySO_3H$, all ligands were commercially purchased and used without further purification. $PySO_3H$ was prepared by a previously reported method.[20]

$[RuCp(CH_3CN)_3]PF_6$ (**1**), $[MoCp(CO)_3]_2$, $[WCp(CO)_3]_2$, $[FeCp(CO)_3]_2$, RhCp(cod), and IrCp(cod) were commercially purchased. Commercial 2-propen-1-ol (AllOH) and synthetic (2-(allyloxy)ethyl)benzene ($C_6H_5CH_2CH_2OAll$ (**2**))[21] were purified by distillation and stored in a Schlenk flask under Ar.

*4.2.2. Ligand screening in **Fig. 3***

The Chemspeed ASW2000 (single syringe) system was customized for use under an inert atmosphere (see Supplementary Data), and Chemspeed-G735 software was used to program the screening. Five sets of reaction blocks**,** each containing 16 glass vials, were heated at 120 °C for 30 min under a reduced pressure of 200 mmHg. To each of 48 vials, ligands L1-L48 (each 5.00 μmol) were manually added within a glovebox, and the temperature of the five reaction blocks was adjusted to 30 °C. A 10.0 mM stock solution of $[RuCp(CH_3CN)_3]PF_6$ (**1**) in CH_3OH (30 mL), and three 111 mM stock solutions of $C_6H_5CH_2CH_2OAll$ (**2**) (80 mL x 3) were prepared in four 100-mL vials in a storage tray. A 500-μL aliquot of solution **1** (5.00 μmol) was first added to each 20-mL reaction vessel, and then the single syringe needle was subjected to a 20-sec outside/inside rinse with CH_3OH. Next, a 4.50-mL aliquot of solution **2** (500 μmol) was added to each of the vessels. All other reactions (L2–L48) were prepared in this way, taking ca. 1 h. After being shaken at 30 °C for 3 h from the start point of the first reaction (L1), the glovebox-type hood was opened, and a 200 μL aliquot of the reaction mixture (L1) was placed in a 5-mL vial of a sampling tray, and the syringe was cleaned by a 20-sec outside/inside rinse with CH_3OH. The sample was manually frozen by using liquid N_2. All other samples, which were consecutively transferred from the corresponding reaction vessels every 75 sec, were frozen. Gas chromatography analyses of the samples were performed on Shimazu GC-14B and GC-17A instruments with the following conditions: capillary column, J&W Scientific DB-WAX (0.25 mm x 15 m); column temperature, 50–250 °C; rate of temperature increase, 10 °C/min; t_R 4.0 min (**2**) and 6.0 min (**3**).

4.2.3. Ligand optimization in Tables 1 and 2

All reactions were carried out under Ar atmosphere by using a general Schlenk technique. Schlenk flasks were dried at ca. 250 °C by using a heat gun under reduced pressure, and a Teflon-coated magnetic bar was used to stir the reaction mixture. The typical procedure is represented by the reaction of entry 1 in **Table 1**: $[RuCp(CH_3CN)_3]PF_6$ (**1**) (1.60 mg, 3.69 μmol) and CH_3OH (0.330 mL) were placed in a 20-mL Schlenk tube under Ar stream. A 100 mM solution of PAH (0.0370 mL, 37.0 μmol) in CH_3OH was added to the mixture. After standing for 30 min at rt, the reddish brown solution was transferred into a 20-mL Schlenk tube equipped with a Young's tap containing $C_6H_5CH_2CH_2OAll$ (**2**) (300 mg, 1.85 mmol) and CH_3OH (3.00 mL). The yellow solution was stirred for 1 h at 30 °C. GC analysis (conditions as above) was used to determine the yield of $C_6H_5CH_2CH_2OH$ (**3**). Instead of **1** and PAH, other CpM precursors and ligands were used.

4.3. NMR experiments

A dry and Ar-filled 5-mm Young-type NMR tube was charged with a 200-mM $(CD_3)_2CO$ solution of QAH (0.500 mL, 100 μmol), and subjected to ^{1}H-NMR analysis at 30 °C (**Fig. 7a**). After degassing the mixture by two freeze/thaw cycles, a 200-mM $(CD_3)_2CO$ solution of $[RuCp(CH_3CN)_3]PF_6$ (**1**) (0.500 mL, 100 μmol) was added to the NMR tube under Ar atmosphere. After 10 min at 30 °C, the ^{1}H-NMR spectrum was recorded (**Fig. 7b**), and then a 500-mM $(CD_3)_2CO$ solution of $C_6H_5CH_2CH_2OAll$ (**2**) (0.200 mL, 100 μmol) was added. After 30 min at 30 °C, the ^{1}H-NMR spectrum was recorded (**Fig. 7c**), and then **2** (162 mg, 1.00 mmol) and CH_3OH (405 μL, 320 mg, 10.0 mmol) were added. After 12 h at 30 °C, the final ^{1}H-NMR spectrum was recorded (**Fig. 7d**). In a separate experiment, a 1:1 mixture of the deprotected alcohol, $C_6H_5CH_2CH_2OH$ (**3**), and the co-product, CH_3OAll, showed OCH_2 signals in a ca. 1:0.5 ratio.

4.4. Kinetic experiments

The allyl ether substrate $C_6H_5CH_2CH_2OAll$ (**2**) and air- and moisture-stable $[RuCp(\eta^3\text{-}C_3H_5)(QA)]PF_6$ (**5**) were used for the kinetic study. Three stock solutions of **2** in CD_3OD at 333 mM (S-**I**), 556 mM (S-**II**), and 1.11 M (S-**III**), and three stock solutions of **5** in CD_3OD at 5.00 mM (C-**I**), 10.0 mM (C-**II**), and 20.0 mM (C-**III**) were prepared in advance, and degassed by three freeze/thaw cycles. Five dried and Ar-filled 5-mm Young-type NMR tubes were charged, respectively, with S-**I** (900 μL, 300 μmol **2**), three lots of S-**II** (900 μL, 500 μmol **2**), and S-**III** (900 μL, 1.00 mmol **2**), and then immersed in a dry ice/CH_3OH bath. To these tubes were added, C-**I** (100 μL, 0.500 μmol **5**), three lots of C-**II** (100 μL, 1.00 μmol), and C-**III** (100 μL, 2.00 μmol). Each of the five cooled S-**I**/C-**II**, S-**II**/C-**II**, S-**III**/C-**II**, S-**II**/C-**I**, S-**II**/C-**II** combined systems was measured by ^{1}H-NMR with the probe temperature adjusted to 30 °C. FID was sampled every 5 min for 3 h. The signal intensity at δ 3.77 (2H, t, J = 7.57 Hz, $C_6H_5CH_2CH_2OH$ (**3**)) was plotted over time, and the rate was determined in the 0%–30% conversion range.[15] In the early reaction stage, logarithmic plotting afforded high linearity to determine the following initial rates: 12.2 mM/min (S-**I**/C-**II**), 12.4 mM/min (S-**II**/C-**II**), 12.6 mM/min (S-**III**/C-**II**), 8.32 mM/min (S-**II**/C-**I**), and 26.3 mM/min (S-**II**/C-**II**).

4.5. Preparation of metal complexes and X-ray crystallographic analysis

4.5.1. $[RuCp(\eta^3\text{-}C_3H_5)(4\text{-}CH_3O\text{-}PA)]PF_6$

A dry and Ar-filled 10-mL Schlenk flask was charged with $[RuCp(CH_3CN)_3]PF_6$ (**1**) (3.21 mg, 73.9 μmol), 4-CH_3O-PAH (11.3 mg, 73.8 μmol), and $(CH_3)_2CO$ (7.0 mL) at rt. After the resulting yellow solution was stirred at rt for 5 min, a 200-mM $(CH_3)_2CO$ solution of AllOH (369 μL, 73.7 μmol) was introduced to the Schlenk flask. The resulting purple solution was cannulated into a 5-mL tube placed in a 20-mL Schlenk

flask, and hexane (3.0 mL) was added to the Schlenk flask outside the 5-mL tube. After sealing the system by using a silicone-greased glass stopper, the whole system was kept at 5 °C for 12 h to generate yellow prismatic crystals (32.0 mg, 63.5 μmol, 86% yield): ^{1}H NMR ($(CD_3)_2CO$) δ 4.09 (s, 3H, OCH_3), 4.23 (dd, J = 6.54, 2.75 Hz, 1H, CH_{syn}), 4.39 (dd, J = 6.20, 2.75 Hz, 1H, CH_{syn}), 4.46 (d, J = 11.02 Hz, 1H, CH_{anti}), 4.60 (d, J = 11.02 Hz, 1H, CH_{anti}), 4.86 (dddd, J = 11.02, 11.02, 6.20, 6.20 Hz, 1H, CH_{center}), 6.36 (s, 5H, Cp), 7.40 (dd, J = 6.54, 2.75 Hz, 1H, C(5)H), 7.45 (d, J = 2.75 Hz, 1H, C(3)H), 8.81 (d, J = 6.89 Hz, 1H, C(6)H); ^{13}C NMR ($(CD_3)_2CO$) δ 57.7, 66.3, 68.4, 97.1, 101.8, 114.2, 116.7, 152.4, 158.4, 170.8, 171.1; HRMS (ESI) m/z: calcd for $C_{15}H_{16}NO_3Ru$ $[M–PF_6]^+$, 360.0174; found, 360.0174; mp 186 °C (decomposed).

Crystallographic data for the structures in this paper have been deposited with the Cambridge Crystallographic Data Centre. Copies of the data can be obtained, free of charge, on application to CCDC, 12 Union Road, Cambridge CB2 1EZ, UK (fax: +44-(0)1223-336033 or e-mail: deposit@ccdc.cam.ac.Uk). RuCp(η^3-C_3H_5)(4-CH_3O-PA)]PF_6 is available as supplementary publication no. CCDC 1052811. Crystals of [RuCp(η^3-C_3H_5)(PA)]PF_6, [RuCp(η^3-C_3H_5)(4-Cl-PA)]PF_6, [RuCp(η^3-C_3H_5)(4-CF_3-PA)]PF_6, and [RuCp(η^3-C_3H_5)(4-NO_2-PA)]PF_6 were prepared in the same way.

4.5.2. [RuCp(η^3-C_3H_5)(PA)]PF_6

Conditions: [RuCp(CH_3CN)$_3$]PF_6 (**1**) (32.0 mg, 73.7 μmol), PAH (9.01 mg, 73.2 μmol), $(CH_3)_2CO$ (7.00 mL), a 200-mM $(CH_3)_2CO$ solution of AllOH (369 μL, 73.7 μmol). [RuCp(η^3-C_3H_5)(PA)]PF_6 (31.3 mg, 66.0 μmol, 90% yield) as yellow prismatic crystals: ^{1}H NMR ($(CD_3)_2CO$) δ 4.27 (dd, J = 6.54, 2.75 Hz, 1H, CH_{syn}), 4.45 (dd, J = 6.20, 2.75 Hz, 1H, CH_{syn}), 4.50 (d, J = 11.02 Hz, CH_{anti}), 4.66 (d, J = 10.33 Hz, 1H, CH_{anti}), 4.94 (dddd, J = 11.02, 11.02, 6.20, 6.20 Hz, 1H, CH_{center}), 6.39 (s, 5H, Cp), 7.89 (dd, J = 6.89, 6.20 Hz, C(5)H), 7.99 (d, J = 8.26 Hz, 1H, C(3)H), 8.35 (dd, J = 7.57, 7.57 Hz, 1H, C(4)H), 9.08 (d, J = 5.51 Hz, 1H, C(6)H); ^{13}C NMR ($(CD_3)_2CO$) δ 66.4, 69.3, 97.4, 101.9, 128.9, 130.5, 142.9, 151.0, 158.2, 171.3; HRMS (ESI) m/z: calcd for $C_{14}H_{14}NO_2Ru$ $[M–PF_6]^+$, 330.0068; found, 330.0090; mp 210 °C (decomposed). Crystallographic data no. CCDC 1052813.

4.5.3. [RuCp(η^3-C_3H_5)(4-Cl-PA)]PF_6

Conditions: [RuCp(CH_3CN)$_3$]PF_6 (**1**) (32.2 mg, 74.1 μmol), 4-Cl-PAH (11.6 mg, 73.7 μmol), $(CH_3)_2CO$ (7.0 mL), a 200-mM $(CH_3)_2CO$ solution of AllOH (369 μL, 73.7 μmol). [RuCp(η^3-C_3H_5)(4-Cl-PA)]PF_6 (37.5 mg, 60.1 μmol, 82% yield) as yellow prismatic crystals: ^{1}H NMR ($(CD_3)_2CO$) δ 4.29 (dd, J = 6.89, 2.75 Hz, 1H, CH_{syn}), 4.48 (dd, J = 6.20, 2.75 Hz, 1H, CH_{syn}), 4.52 (d, J = 11.02 Hz, 1H, CH_{anti}), 4.69 (d, J = 11.02 Hz, 1H, CH_{anti}), 5.02 (dddd, J = 11.02, 11.02, 6.89, 6.20 Hz, 1H, CH_{center}), 6.41 (s, 5H, Cp), 7.96 (d, J = 2.75 Hz, 1H, C(3)H), 8.00 (dd, J = 6.20, 2.75 Hz, 1H, C(5)H), 9.05 (d, J = 6.20 Hz, 1H, C(6)H); ^{13}C NMR ($(CD_3)_2CO$) δ 66.6, 69.6, 97.4, 102.1, 128.7, 130.4, 150.7, 152.2, 158.8, 170.3; HRMS (ESI) m/z: calcd for $C_{14}H_{13}ClNO_2Ru$ $[M–PF_6]^+$, 363.9678; found, 363.9703; mp 216 °C (decomposed). Crystallographic data no. CCDC 1052810.

4.5.4. [RuCp(η^3-C_3H_5)(4-CF_3-PA)]PF_6

Conditions: [RuCp(CH_3CN)$_3$]PF_6 (**1**) (32.1 mg, 73.9 μmol), 4-CF_3-PAH (14.1 mg, 73.8 μmol), $(CH_3)_2CO$ (7.0 mL), a 200-mM $(CH_3)_2CO$ solution of AllOH (369 μL, 73.7 μmol). [RuCp(η^3-C_3H_5)(4-CF_3-PA)]PF_6 (30.1 mg, 55.6 μmol, 75% yield) as yellow prismatic crystals: ^{1}H NMR ($(CD_3)_2CO$) δ 4.34 (dd, J = 6.46, 2.75 Hz, 1H, CH_{syn}), 4.53 (dd, J = 5.93, 2.75 Hz, 1H, CH_{syn}), 4.56 (d, J = 11.02 Hz, 1H, CH_{anti}), 4.75 (d, J = 11.02 Hz, 1H, CH_{anti}), 5.07 (dddd, J = 11.02, 11.02, 6.89, 6.20 Hz, 1H, CH_{center}), 6.43 (s, 5H, Cp), 8.15 (d, J = 2.07 Hz, 1H, C(3)H), 8.23 (dd, J = 5.51, 2.07 Hz, 1H, C(5)H), 9.40 (d, J = 6.20 Hz, 1H, C(6)H); ^{13}C NMR ($(CD_3)_2CO$) δ 66.7, 70.2, 97.5, 102.2, 124.2, 126.1, 142.9 (q, J = 141.4 Hz), 152.9 (2C), 160.0, 170.2; HRMS (ESI) m/z: calcd for $C_{15}H_{13}F_3NO_2Ru$ $[M–PF_6]^+$, 397.9942; found, 397.9968; mp 182 °C (decomposed). Crystallographic data no. CCDC 1052809.

4.5.5. [RuCp(η^3-C_3H_5)(4-NO_2-PA)]PF_6

Conditions: [RuCp(CH_3CN)$_3$]PF_6 (**1**) (32.0 mg, 73.7 μmol), 4-NO_2-PAH (12.4 mg, 73.8 μmol), $(CH_3)_2CO$ (7.0 mL), a 200-mM $(CH_3)_2CO$ solution of AllOH (369 μL, 73.7 μmol). [RuCp(η^3-C_3H_5)(4-NO_2-PA)]PF_6 (22.2 mg, 42.8 μmol, 58% yield) as yellow prismatic crystals: ^{1}H NMR ($(CD_3)_2CO$) δ 4.37 (dd, J = 6.54, 2.75 Hz, 1H, CH_{syn}), 4.55 (dd, J = 6.20, 2.75 Hz, 1H, CH_{syn}), 4.60 (d, J = 11.02 Hz, 1H, CH_{anti}), 4.78 (d, J = 11.02 Hz, 1H, CH_{anti}), 5.09 (dddd, J = 11.71, 11.02, 6.89, 6.20 Hz, 1H, CH_{center}), 6.46 (s, 5H, Cp), 8.43 (d, J = 2.75 Hz, 1H, C(3)H), 8.56 (dd, J = 6.20, 2.75 Hz, 1H, C(5)H), 9.53 (d, J = 6.20 Hz, 1H, C(6)H); ^{13}C NMR ($(CD_3)_2CO$) δ 66.8, 70.7, 97.6, 102.4, 121.0, 122.9, 154.3, 157.8, 161.1, 169.8; HRMS (ESI) m/z: calcd for $C_{14}H_{13}N_2O_4Ru$ $[M–PF_6]^+$, 374.9919; found, 374.9933; mp 172 °C (decomposed). Crystallographic data no. CCDC 1052812.

Acknowledgments

This work was supported by a Grant-in-Aid for Scientific Research (No. 25410112, 24106713) and Platform for Drug Discovery, Informatics, and Structural Life Science from the Ministry of Education, Culture, Sports, Science and Technology (Japan), and an Advanced Catalytic Transformation Program for Carbon Utilization (ACT-C) from Japan Science and Technology Agency (JST).

References and notes

1. (a) *Protective Groups in Organic Synthesis*, 3rd ed.; Greene, T. W., Wuts, P. G. M., Eds.; Wiley-VCH: New York, U.S.A., 2000; (b) Schelhaas, M.; Waldmann, H. *Angew. Chem., Int. Ed. Engl.* **1996**, *35*, 2056.
2. Corey, E. J.; Suggs, J. W. *J. Org. Chem.* **1973**, *38*, 3224.
3. (a) Oltvoort, J. J.; van Boeckel, C. A. A.; de Koning, J. H.; van Boom, J. H. *Synthesis* **1981**, 305; For other isomerization-based methods, see: (b) Cadot, C.; Dalko, P. I.; Cossy, J. *Tetrahedron Lett.* **2002**, 43, 1839; (b) Nicolaou, K. C.; Hummel, C. W.; Bockovich, N. J.; Wong, C.-H. *J. Chem. Soc., Chem. Commun.* **1991**, 870; (c) Boss, R.; Scheffold, R. *Angew. Chem., Int. Ed. Engl.* **1976**, *15*, 558; (d) Cunningham, J.; Gigg, R.; Warren, C. D. *Tetrahedron Lett.* **1964**, 1191.
4. (a) Vutukuri, D. R.; Bharathi, P.; Yu, Z.; Rajasekaran, K.; Tran, M.-H.; Thayumanavan, S. *J. Org. Chem.* **2003**, *68*, 1146; (b) Chandrasekhar, S.; Reddy, C. R.; Rao, R. J. *Tetrahedron* **2001**, *57*, 3435; (c) Honda, M.; Morita, H.; Nagakura, I. *J. Org. Chem.* **1997**, *62*, 8932; (d) Beugelmans, R.; Bourdet, S.; Bigot, A.; Zhu, J. *Tetrahedron Lett.* **1994**, *35*, 4349.
5. Taniguchi, T.; Ogasawara, K. *Angew. Chem., Int. Ed.* **1998**, *37*, 1136.
6. Kitov, P. I.; Bundle, D. R. *Org. Lett.* **2001**, *3*, 2835.
7. (a) Tanaka, S.; Saburi, H.; Ishibashi, Y.; Kitamura, M. *Org. Lett.* **2004**, *6*, 1873; (b) Saburi, H.; Tanaka, S.; Kitamura, M. *Angew. Chem., Int. Ed.* **2005**, *44*, 1730; (c) Tanaka, S.; Saburi, H.; Kitamura, M. *Adv. Synth. Catal.* **2006**, *348*, 375; (d) Tanaka, S.; Saburi, H.; Murase, T.; Yoshimura, M.; Kitamura, M. *J. Org. Chem.* **2006**, *71*, 4682; (e) Tanaka, S.; Saburi, H.; Murase, T.; Ishibashi, Y.; Kitamura, M. *J. Organomet. Chem.* **2007**, *692*, 295; (f) Tanaka, S.; Hirakawa, T.; Oishi, K.; Hayakawa, Y.; Kitamura, M. *Tetrahedron Lett.* **2007**, *48*, 7320; (g) Tanaka, S.; Saburi, H.; Hirakawa, T.; Seki, T.; Kitamura, M. *Chem. Lett.* **2009**, *38*, 188; (h) Hirakawa, T.; Tanaka, S.; Usuki, N.; Kanzaki, H.; Kishimoto, M.; Kitamura, M. *Eur. J. Org. Chem.* **2009**, 789–792.
8. (a) Noyori, R.; Kitamura, M. *Angew. Chem., Int. Ed. Engl.* **1991**, *30*, 49–69; For the original reaction deducing Intramol-MDACat

concept, see: (b) Kitamura, M.; Suga, S.; Kawai, K.; Noyori, R. *J. Am. Chem. Soc.* **1986**, *108*, 6071-6072.

9. Some examples for hydrogenation: (a) Ohkuma, T.; Ooka, H.; Hashiguchi, S.; Ikariya, T.; Noyori, R. *J. Am. Chem. Soc.* **1995**, *117*, 2675; (b) Noyori R.; Ohkuma, T. *Angew. Chem., Int. Ed.* **2001**, *40*, 40; (c) H. Huang, T. Okuno, K. Tsuda, M. Yoshimura, M. Kitamura, *J. Am. Chem. Soc.* **2006**, *128*, 8716–8717; (d) Yamamura, T.; Nakatsuka, H.; Tanaka, S.; Kitamura, M. *Angew. Chem. Int. Ed*. **2013**, *52*, 1; Transfer hydrogenation: (e) Hashiguchi, S.; Fujii, A.; Takehara, J.; Ikariya, T.; Noyori, R. *J. Am. Chem. Soc.* **1995**, *117*, 7562.
10. (a) Nakano, K.; Bessho, Y.; Kitamura, M. *Chem. Lett.* **2003**, *32*, 224; (b) Kitamura, M.; Miki, T.; Nakano, K.; Noyori, R. *Bull. Chem. Soc. Jpn.* **2000**, *73*, 999.
11. Bifunctional Molecular Catalysis; Ikariya, T., Shibasaki, M., Eds.; Springer: Heidelberg, Germany, 2011.
12. (a) Noyori, R.; Kitamura, M.; Ohkuma, T. *Proc. Natl. Acad. Sci. U. S. A.* **2004**, 101, 5356; (b) Kitamura, M.; Nakatsuka, H. *Chem. Commun.* **2011**, *47*, 842. For the original reaction deducing Intermol-MDACat, see: (c) Noyori, R.; Ohkuma, T.; Kitamura, M.; Takaya, H.; Sayo, N.; Kumobayashi, H.; Akutagawa, S. *J. Am. Chem. Soc.* **1987**, *109*, 5856; (d) Kitamura, M.; Ohkuma, T.; Inoue, S.; Sayo, N.; Kumobayashi, H.; Akutagawa, S.; Ohta, T.; Takaya, H.; Noyori, R. *J. Am. Chem. Soc*. **1988**, *110*, 629.
13. (a) Kitamura, M.; Tanaka, S.; Yoshimura, M. *J. Org. Chem*. **2002**, *67*, 4975–4977; For the first report on the utility or Cp*Ru complex in π -allyl chemistry, see: (b) Kondo, T.; Ono, H.; Satake, N.; Mitsudo, T.; Watanabe, Y. *Organometallics* **1995**, *14*, 1945; For the subsequent related reports, see: (c) Trost, B. M.; Fraisse, P. L.; Ball, Z. T. *Angew. Chem., Int. Ed.* **2002**, *41*, 1059; (d) Mbaye, M. D.; Demerseman, B.; Renaud, J.-L.; Toupet, L.; Bruneau, C. *Angew. Chem., Int. Ed*. **2003**, *42*, 5066; (e) Burger, E. C.; Tunge, J. A. *Org. Lett*. **2004**, *6*, 2603; (f) Hermatschweiler, R.; Fernández, I.; Breher, F.; Pregosin, P. S.; Veiros, L. F.; Calhorda, M. J. *Angew. Chem., Int. Ed.* **2005**, *44*, 4397.
14. Books for automated synthesis and catalyst screening: (a) *Applied Homogeneous Catalysis*; Behr, A., Neubert, P., Eds.; Wiley-VCH: Weinheim, Germany, 2012; (b) *Micro Instrumentation for High Throughpur Experimentation and Process Intensification–a Tool of PAT*; Koch, M. V., VandenBussche, K. M., Chrisman, R. W., Eds.; Wiley-VCH: Weinheim, Germany, 2007; (c) *Principles and Methods for Accelerated Catalyst Design and Testing*; Derouane, E.G., Parmon, V., Lemos, F., Ribeiro, F. R., Eds.; Kluwer Academic Publishers: Dordrecht, 2002.
15. For details, see supplementary data.
16. Wuu, Y.-M.; Wrighton, M. S. *Organometallics* **1988**, *7*, 1839.
17. *Dictionary of Organic Compounds*, 6th ed. vol. 6; Buckingham, J., Macdonald, F., Eds.; Chapman & Hall: London, UK, 1996.
18. Some examples of asymmetric allylation established on the basis of RDACat concept: (a) Miyata, K.; Kutsuna, H.; Kawakami, S.; Kitamura, M. *Angew. Chem., Int. Ed*. **2011**, *50*, 4649; Tanaka, T. Seki, M. Kitamura. *Angew. Chem., Int. Ed*. **2009**, *48*, 8948; (c) Seki, T.; Tanaka, S.; Kitamura, M. *Org. Lett*. **2012**, *14*, 608; (d) Miyata, K.; Kitamura, M. *Synthesis* **2012**, *44*, 2138; (e) Kitamura, M.; Miyata, K.; Seki, T.; Vatmurge, N.; Tanaka, S. *Pure Appl. Chem*. **2013**, *85*, 1121.
19. Refosco, F.; Tisato, F.; Bandoli, G.; Deutsch, E. *J. Chem. Soc., Dalton Trans.* **1993**, 2901–2908.
20. den Hertog, H. J.; van der Plas, H. C.; Buurman, D. J. *Recueil* **1958**, *77*, 963–972.
21. Hill, C. M.; Simmons, D. E.; Hill, M. E. *J. Am. Chem. Soc.* **1955**, *77*, 3889–3892.

Supplementary Material

Supplementary data associated with this article can be found in the online version at dx.doi.org—j.tet.2015.XX.XXX. These data include details of the customized Chemspeed system, the original time-conversion curves for kinetic analysis, and the X-ray crystallographic analyses. The X-ray diffraction data can be obtained free of charge from the Cambridge Crystallographic Data Centre via www.ccdc.cam.ac.uk—data_re-quest/cif.

Supplementary Data

Soft Ruthenium and Hard Brønstead Acid Combined Catalyst for Efficient Cleavage of Allyloxy Bonds. Application to Protecting Group Chemistry.

*Shinji Tanaka, Yusuke Suzuki, Hajime Saburi, and Masato Kitamura**

Contents

1. Customized Chemspeed ASW2000

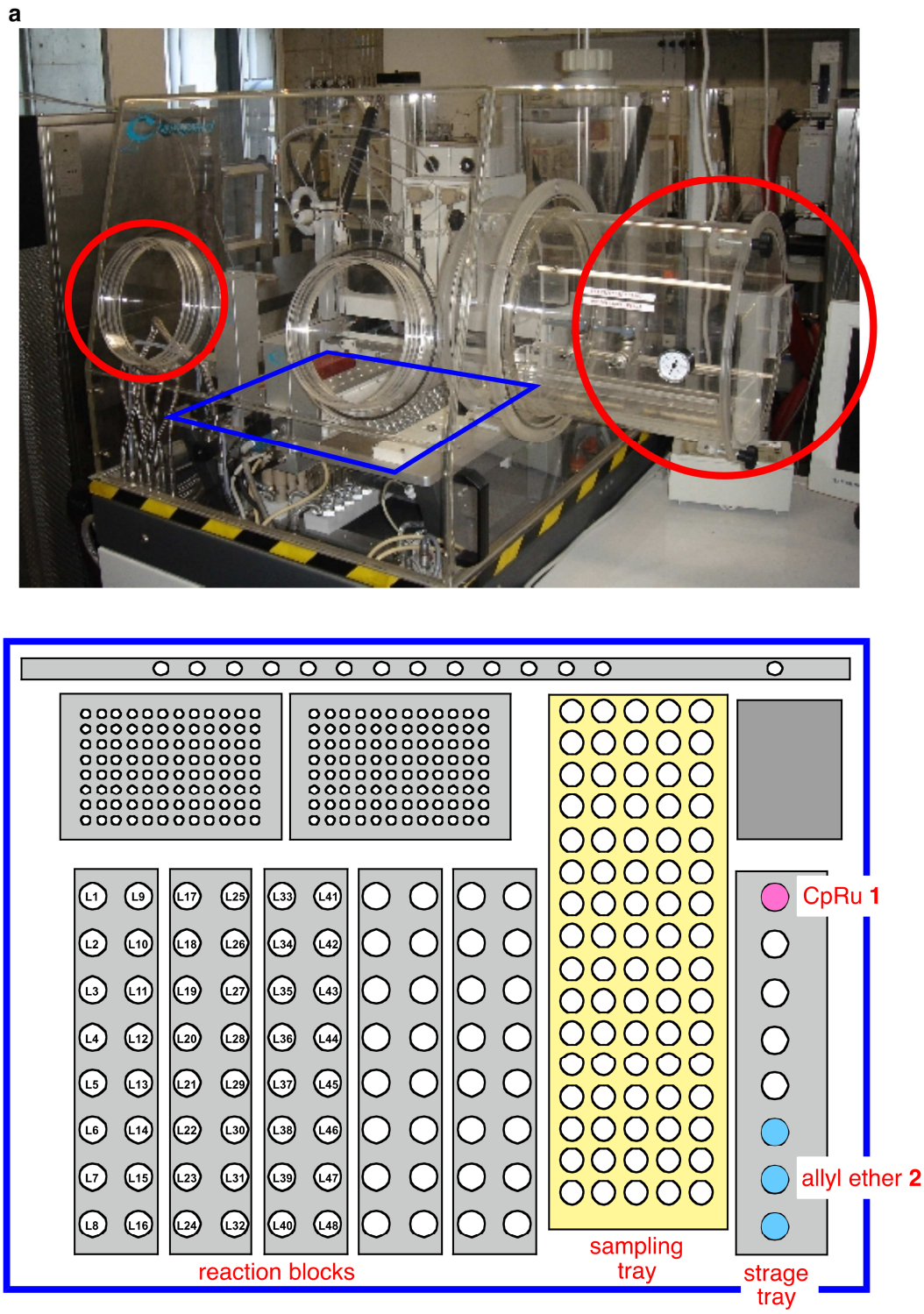

Figure S1. Chemspeed ASW2000 equipped with a glovebox-type hood (a) and the structures of L1–L48 screened (b).

—Continuation of **Figure S1**—

b

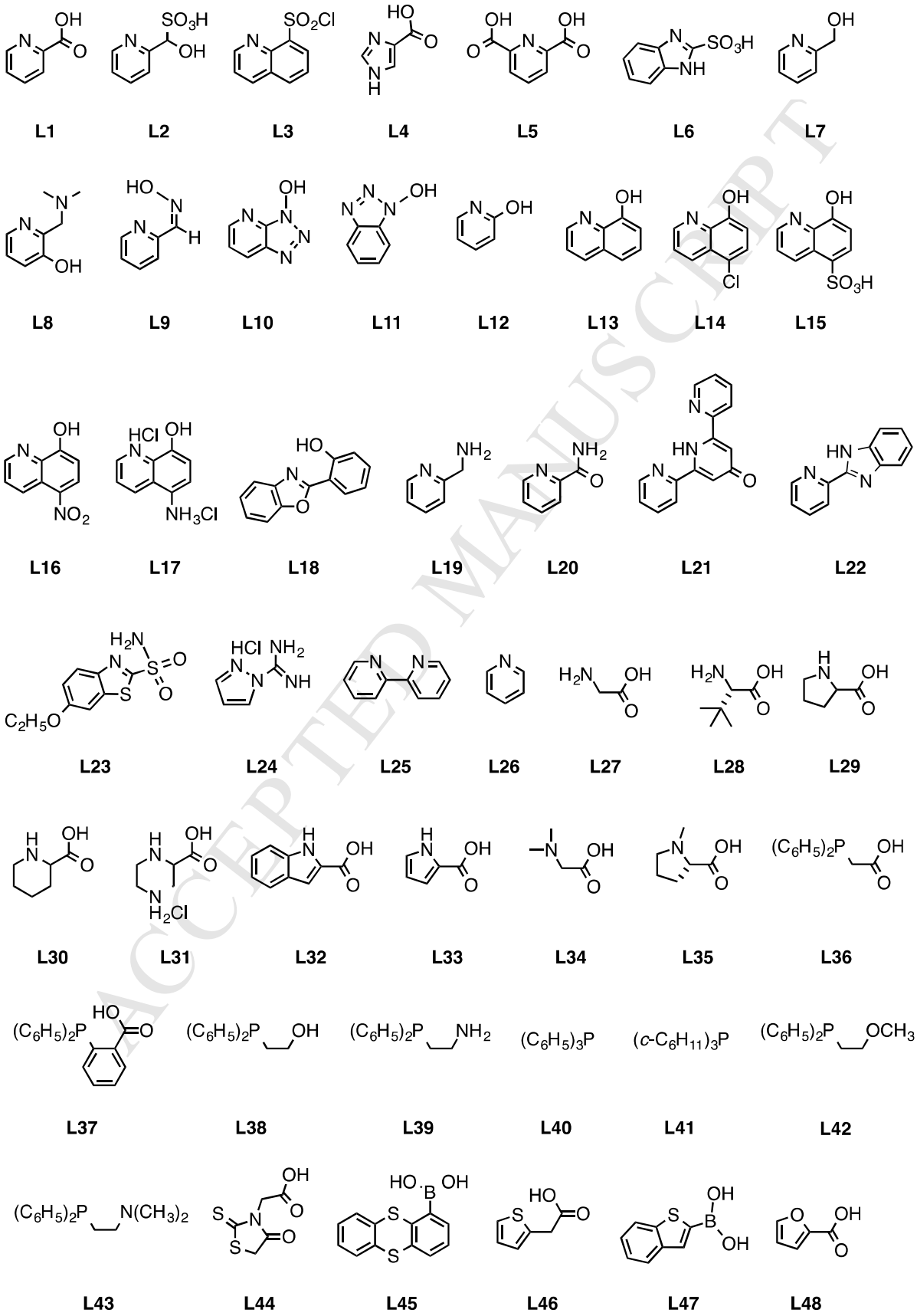

2. Time-conversion curves

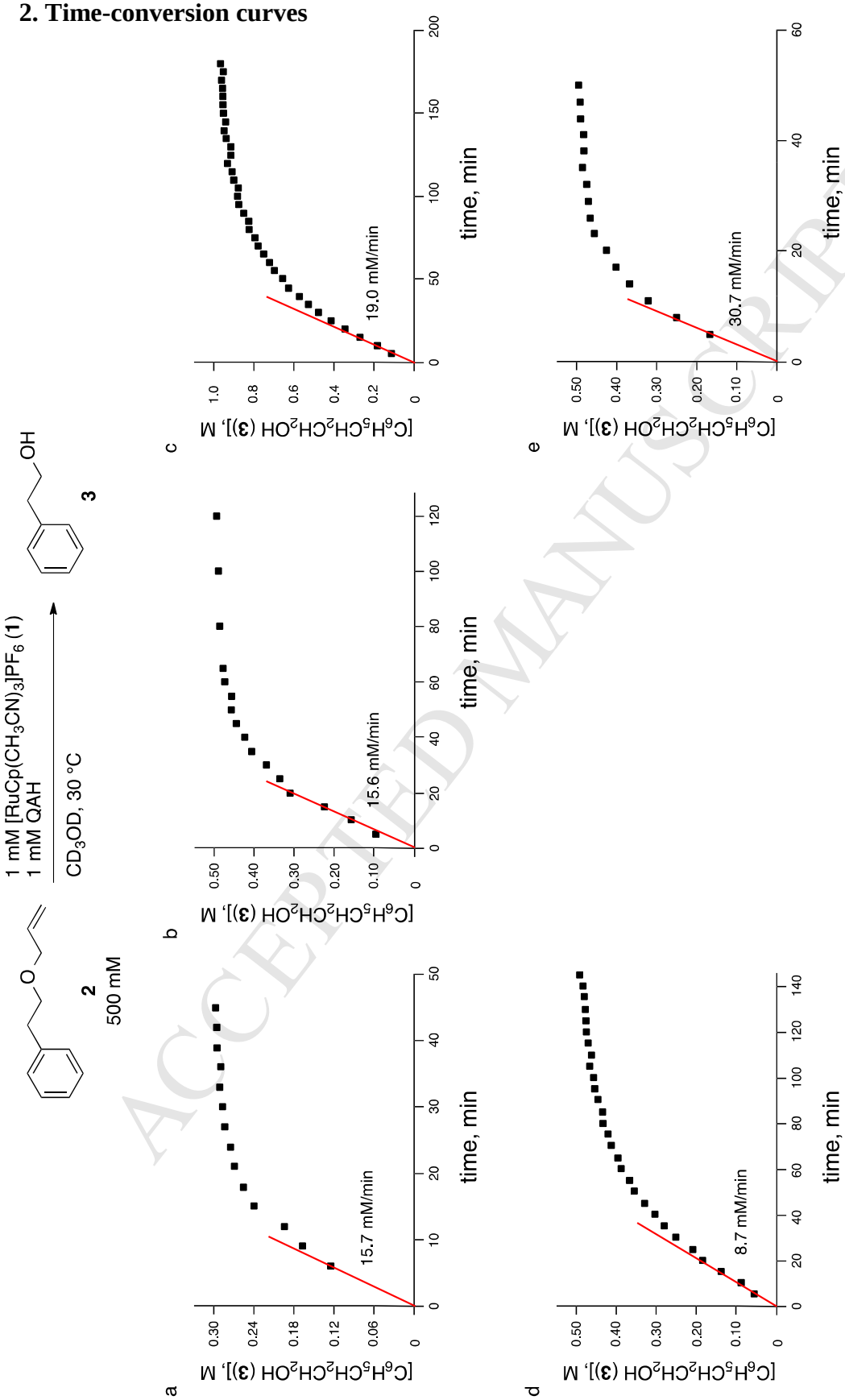

Figure S2. Change in product concentration [$C_6H_5CH_2CH_2OH$ (**3**)] over time in CD_3OD at 30 °C under the following conditions: (a) $[\mathbf{1}]_0$ = $[QAH]_0$ = 1 mM, $[\mathbf{2}]_0$ = 300 mM, (b) $[\mathbf{1}]_0$ = $[QAH]_0$ = 1 mM, $[\mathbf{2}]_0$ = 500 mM, (c) $[\mathbf{1}]_0$ = $[QAH]_0$ = 1 mM, $[\mathbf{2}]_0$ = 1000 mM, (d) $[\mathbf{1}]_0$ = $[QAH]_0$ = 0.5 mM, $[\mathbf{2}]_0$ = 500 mM, and (e) $[\mathbf{1}]_0$ = $[QAH]_0$ = 2 mM, $[2]_0$ = 500 mM.

3. X-ray crystallographic analyses

(a)

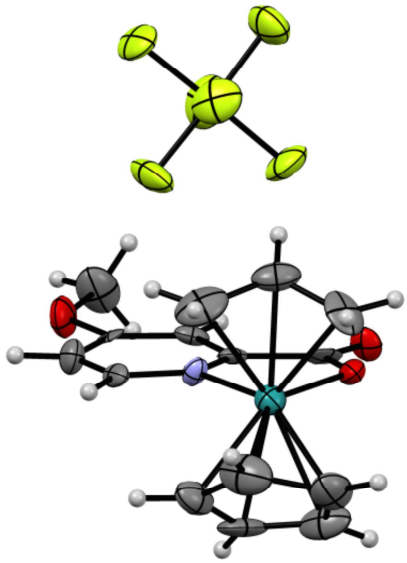

(b)

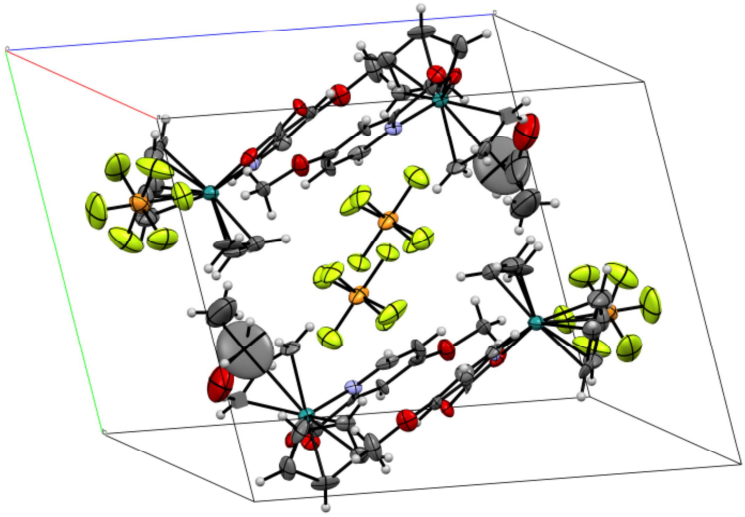

Figure S3. ORTEP drawing of [RuCp(η^3-C_3H_5)(4-CH_3O-PA)]PF_6 (a) and the packing diagram (b).

Table S1. Crystallographic Data and Parameters for $[RuCp(\eta^3\text{-}C_3H_5)(4\text{-}CH_3O\text{-}PA)]PF_6$

mol formula	$C_{15}H_{16}F_6NO_3PRu$
mol wt	504.33
crystal color, habit	yellow, platelet
crystal size, mm^3	0.20 x 0.20 x 0.10
crystal system	triclinic
lattice type	Primitive
space group	*P*–1 (#2)
cell dimens	
a, Å	11.443(5)
b, Å	12.529(5)
c, Å	15.231(6)
α, deg	79.22(1)
β, deg	72.091(13)
γ, deg	84.49(2)
vol, $Å^3$	2039.5(14)
Z	4
ρ calcd, g cm^{-3}	1.766
μ (Mo Kα), cm^{-1}	9.37
diffractometer	Rigaku, Saturn
radiation	Mo Kα (l = 0.71070 Å) graphite monochromated
$2\theta_{max}$, deg	54.9
no. of reflections measured	total: 14698 Unique: 8253 (R_{int} = 0.064)
corrections	Lorentz-polarization
structure solution	Direct methods (SIR92)
function minimized by	$Sw(\lvert F_0\rvert - \lvert F_c\rvert)^2$
refinement	Full-matrix least-squares on F
no. of observations (I>3.00s(I))	2513
no. of variables	562
R	0.047
R_w[a]	0.053
goodness-of-fit Indicator	1.19

[a] $R_w = \{\Sigma\omega(\lvert F_0\rvert - \lvert F_c\rvert)^2/\Sigma\omega F_0^2\}^{1/2}$.

(a)

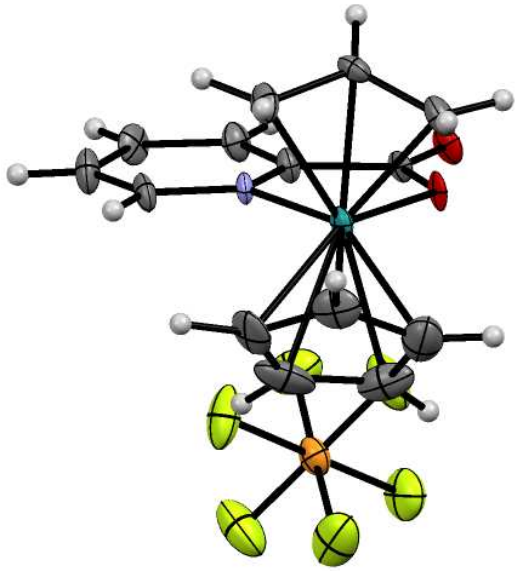

(b)

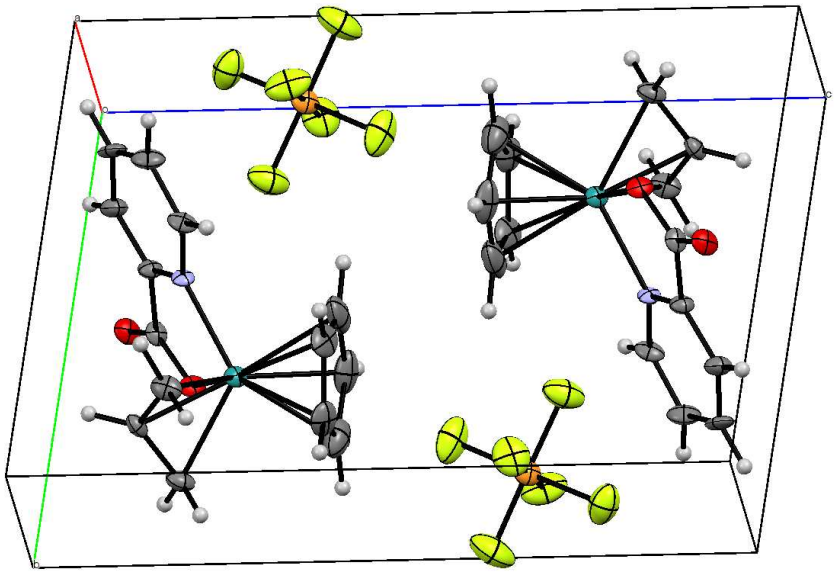

Figure S4. ORTEP drawing of [RuCp(η^3-C_3H_5)(PA)]PF_6 (a) and the packing diagram (b).

Table S2. Crystallographic Data and Parameters for $[RuCp(\eta^3\text{-}C_3H_5)(PA)]PF_6$

mol formula	$C_{14}H_{14}F_6NO_2PRu$
mol wt	474.30
crystal color, habit	yellow, prism
crystal size, mm^3	0.20 x 0.08 x 0.05
crystal system	triclinic
lattice type	Primitive
space group	*P*–1 (#2)
cell dimens	
a, Å	6.939(5)
b, Å	8.628(6)
c, Å	13.539(9)
α, deg	100.651(9)
β, deg	101.600(9)
γ, deg	95.156(10)
vol, $Å^3$	776.5(9)
Z	2
ρ calcd, g cm^{-3}	2.028
μ (Mo Kα), cm^{-1}	11.884
diffractometer	Rigaku, Saturn
radiation	Mo Kα (λ = 0.71075 Å)
	graphite monochromated
$2\theta_{max}$, deg	62.3
no. of reflections measured	total: 7059
	Unique: 4095 (R_{int} = 0.2530)
corrections	Lorentz-polarization
structure solution	Direct methods (SIR92)
function minimized by	$\Sigma\omega(\lvert F_0\rvert - \lvert F_c\rvert)^2$
refinement	Full-matrix least-squares on F^2
no. of observations (I>3.00σ(I))	4095
no. of variables	226
R	0.0952
R_w[a]	0.2384
goodness-of-fit Indicator	1.122

[a] $R_w = \{\Sigma\omega(\lvert F_0\rvert - \lvert F_c\rvert)^2/\Sigma\omega F_0^2\}^{1/2}$.

(a)

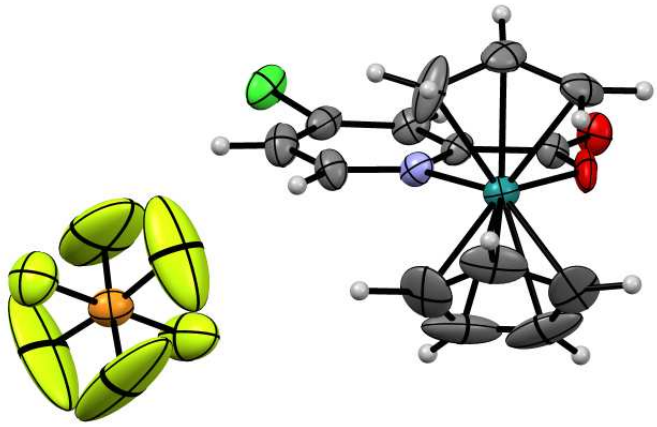

(b)

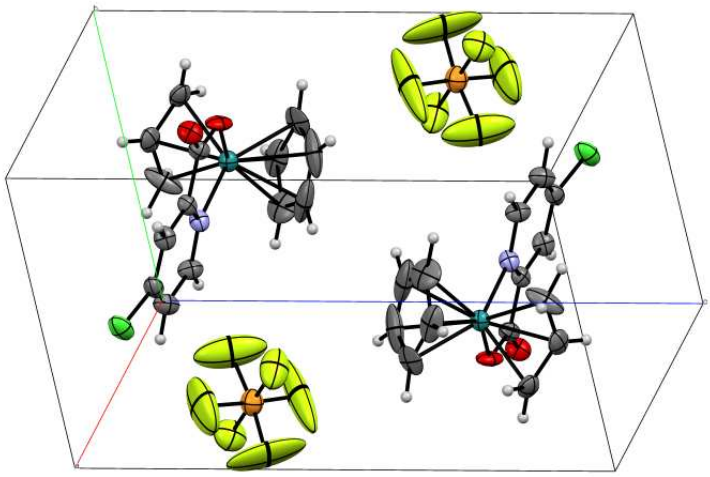

Figure S5. ORTEP drawing of $[RuCp(\eta^3\text{-}C_3H_5)(4\text{-Cl-PA})]PF_6$ (a) and the packing diagram (b).

Table S3. Crystallographic Data and Parameters for $[RuCp(\eta^3\text{-}C_3H_5)(4\text{-}Cl\text{-}PA)]PF_6$

mol formula	$C_{14}H_{13}F_6NO_2PClRu$
mol wt	508.75
crystal color, habit	yellow, prism
crystal size, mm^3	0.10 x 0.10 x 0.10
crystal system	triclinic
lattice type	Primitive
space group	$P\bar{1}$ (#2)
cell dimens	
a, Å	6.969(3)
b, Å	8.911(4)
c, Å	14.038(7)
α, deg	97.912(6)
β, deg	102.973(6)
γ, deg	95.428(6)
vol, $Å^3$	834.3(7)
Z	2
ρ calcd, g cm^{-3}	2.025
μ (Mo Kα), cm^{-1}	12.68
diffractometer	Rigaku, Saturn
radiation	Mo Kα (λ = 0.71070 Å)
	graphite monochromated
$2\theta_{max}$, deg	54.9
no. of reflections measured	total: 5491
	Unique: 3154 (R_{int} = 0.036)
corrections	Lorentz-polarization
structure solution	Direct methods (SIR92)
function minimized by	$\Sigma\omega(\lvert F_0\rvert - \lvert F_c\rvert)^2$
refinement	Full-matrix least-squares on F
no. of observations (I>3.00s(I))	2218
no. of variables	249
R	0.074
R_w[a]	0.077
goodness-of-fit Indicator	2.37

[a] $R_w = \{\Sigma\omega(\lvert F_0\rvert - \lvert F_c\rvert)^2/\Sigma\omega F_0^2\}^{1/2}$.

(a)

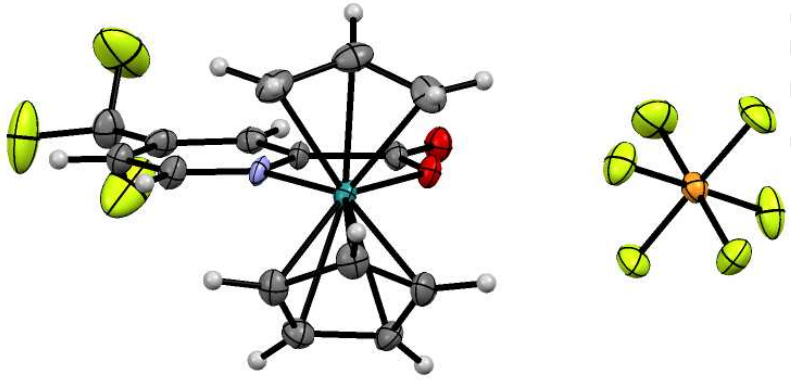

(b)

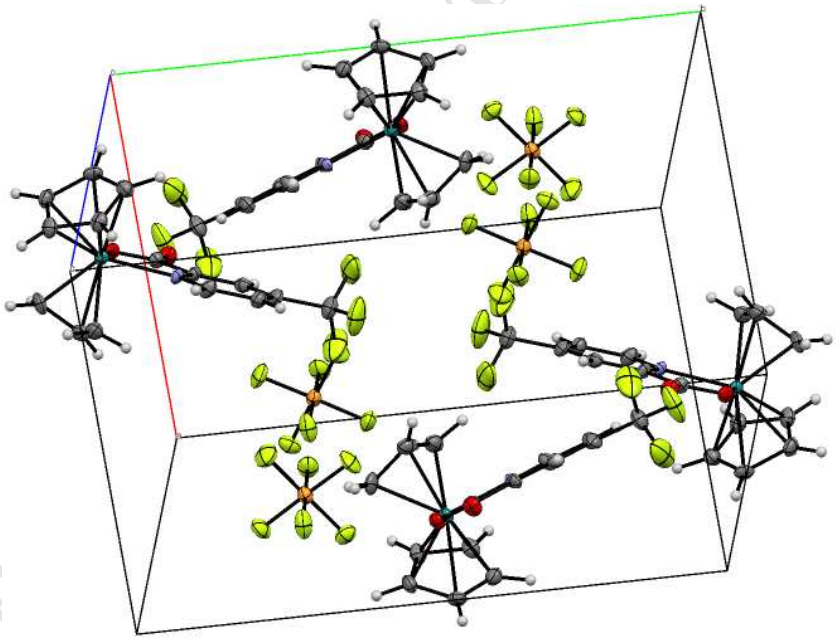

Figure S6. ORTEP drawing of [RuCp(η^3-C_3H_5)(4-CF_3-PA)]PF_6 (a) and the packing diagram (b).

Table S4. Crystallographic Data and Parameters for $[RuCp(\eta^3\text{-}C_3H_5)(4\text{-}CF_3\text{-}PA)]PF_6$

mol formula	$C_{15}H_{13}F_9NO_2PRu$
mol wt	542.30
crystal color, habit	colorless, prism
crystal size, mm^3	0.20 x 0.15 x 0.12
crystal system	monoclinic
lattice type	Primitive
space group	$P2_1/n$ (#14)
cell dimens	
a, Å	11.306(4)
b, Å	16.131(5)
c, Å	13.201(4)
α, deg	90.000
β, deg	95.576(4)
γ, deg	90.000
vol, $Å^3$	2396.0(12)
Z	5
ρ calcd, g cm^{-3}	1.879
μ (Mo Kα), cm^{-1}	9.973
diffractometer	Rigaku, Saturn
radiation	Mo Kα (λ = 0.71075 Å)
	graphite monochromated
$2\theta_{max}$, deg	62.1
no. of reflections measured	total: 20141
	Unique: 6879 (R_{int} = 0.1714)
corrections	Lorentz-polarization
structure solution	Direct methods (SHELX97)
function minimized by	$\Sigma\omega(\lvert F_0\rvert-\lvert F_c\rvert)^2$
refinement	Full-matrix least-squares on F^2
no. of observations (I>3.00s(I))	6879
no. of variables	262
R	0.1196
R_w[a]	0.1247
goodness-of-fit Indicator	1.658

[a] $R_w = \{\Sigma\omega(\lvert F_0\rvert-\lvert F_c\rvert)^2/\Sigma\omega F_0^2\}^{1/2}$.

(a)

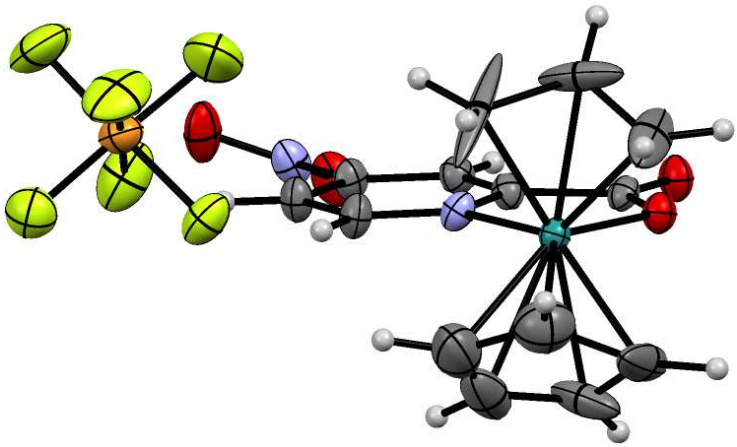

(b)

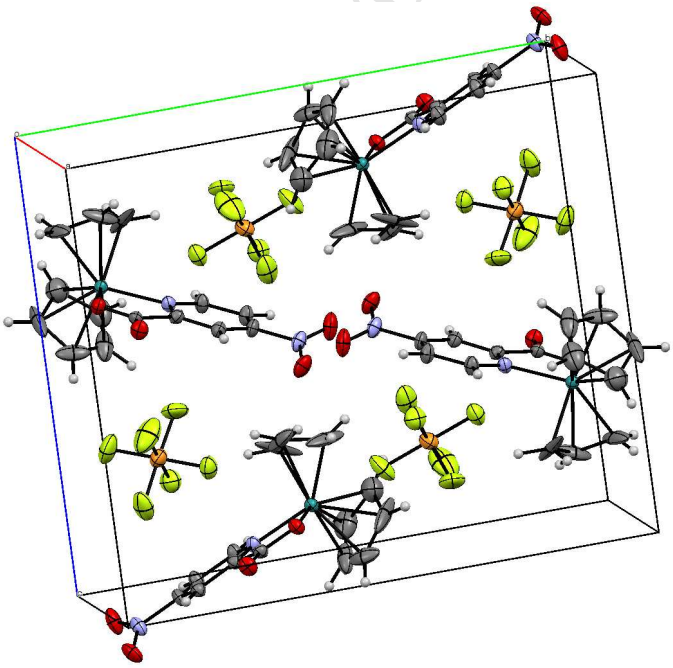

Figure S7. ORTEP drawing of [RuCp(η^3-C_3H_5)(4-NO_2-PA)]PF_6 (a) and the packing diagram (b).

Table S5. Crystallographic Data and Parameters for $[RuCp(\eta^3\text{-}C_3H_5)(4\text{-}NO_2\text{-}PA)]PF_6$

mol formula	$C_{14}H_{13}F_6N_2O_4PRu$
mol wt	532.32
crystal color, habit	orange, prism
crystal size, mm^3	0.11 x 0.08 x 0.05
crystal system	monoclinic
lattice type	Primitive
space group	$P2_1/n$ (#4)
cell dimens	
a, Å	7.274(4)
b, Å	16.296(7)
c, Å	14.155(7)
α, deg	90.0000
β, deg	93.553(6)
g, deg	90.0000
vol, $Å^3$	1674.5(13)
Z	3
ρ calcd, g cm^{-3}	1.584
μ (Mo Kα), cm^{-1}	8.439
diffractometer	Rigaku, Saturn
radiation	Mo Kα (l = 0.71070 Å)
	graphite monochromated
$2\theta_{max}$, deg	62.4
no. of reflections measured	total: 14220
	Unique: 4814 (R_{int} = 0.1635)
corrections	Lorentz-polarization
structure solution	Direct methods (SHELX97)
function minimized by	$\Sigma\omega(\lvert F_0\rvert-\lvert F_c\rvert)^2$
refinement	Full-matrix least-squares on F^2
no. of observations (I>3.00*s*(I))	4814
no. of variables	253
R	0.0877
R_w[a]	0.0986
goodness-of-fit Indicator	1.090

[a] $R_w = \{\Sigma\omega(\lvert F_0\rvert-\lvert F_c\rvert)^2/\Sigma\omega F_0^2\}^{1/2}$.